Magnetic and Optical Properties of Trigonal Zigzag Graphene Nanodisks

The ground state calculations have been performed to check whether the results obtained with the PPP model (which has long-range Coulomb interactions, in addition to the on-site Coulomb repulsion U of the Hubbard model) are consistent with those of Lieb's theorem valid for the Hubbard model. Our calculated total CI energies for various spin multiplicities of the disks predict the triplet state to be lower in energy than the singlet one, for TZGND-2 containing even number of atoms (22), and thus, confirming the validity of Lieb's theorem at the PPP model level. For TZGND-3, for which Lieb's theorem is not strictly valid, our calculations predict contradictory results from the two sets of Coulomb parameters. The low spin state (doublet) is found to be lower in energy (≈ 0.48 eV) than the high spin state (quartet), using the screened parameters, while the standard ones predict the energy difference between the two spin states as ≈ 0.08 eV. The linear absorption spectra of these nanodisks have also been calculated, to obtain information about the optical signatures of the spin multiplicities of their ground states. At TB level, the calculated absorption spectra, for the case of TZGND-2 and TZGND-3, predict the first peak of very high intensity, located at zero energy. Our absorption calculations performed at CI level are different from those obtained at the TB level as there exists no zero energy peak. Our calculations predict that the first peak has a lesser intensity, and the most intense peak occurs at a higher energy which can be understood as an effect of inclusion of the electron correlations. In this work, we also make a very important prediction for experimentalists which will allow them to detect the spin multiplicities of the ground states of these nanodisks using optical absorption spectroscopy. Based upon our calculations, we predict that at room temperatures, TZGND-2 will be optically transparent till 3 eV. As far as TZGND-3 is concerned, because of the contradictory results regarding the ground state multiplicity obtained using the standard and the screened parameters, the presence (absence) of an absorption peak close to 1 eV will confirm the low spin (high spin) nature of the ground state. In an earlier work from our group, the use of electro-absorption spectroscopy was proposed to determine the

nature of ground state magnetism in zigzag graphene nanoribbons.[1] The distinctive feature of the present work is that, as per our predictions, the ground state spin multiplicity of TZGNDs can be determined without the use of an external electric field.

Graphene has a simple honeycomb structure with zero band gap, and has interesting optoelectronic properties.[2–4] It has been suggested that some graphene nanostructures may possess a tendency towards magnetism, thus, bringing carbon-based magnetism within the realm of possibilities.[5–8] The fact that graphene has no band gap, limits its usage in device applications and other optoelectronic areas, so one way to solve this problem, *i.e.*, to open the band gap, is by synthesizing graphene nanostructures. Hence, there has been a world-wide boom in the research of graphene based nanostructures, such as graphene nanoribbons, graphene quantum dots (GQDs), and their monolayer counterparts, graphene nanodisks (GNDs).[6,9,10] GQDs consist of finite number of carbon atoms arranged in a bipartite lattice, forming different shapes such as triangular, hexagonal, bow-tie or completely irregular shapes etc. with different edge structures, namely zigzag, armchair or mixtures thereof. Triangular shaped GNDs with zigzag edges called trigonal zigzag GNDs (TZGNDs), possess half-filled edge states lying close to the Fermi levels. Theoretically, at non-interacting electron level tight binding (TB) model, these half filled states are present exactly at the Fermi level and have significant charge density concentrated on the edge atoms. It has been argued that the ground states of small TZGNDs exhibit large ferromagnetism (FM) because of the large electron correlation effects amongst the edge states at the Fermi level.[5,11] The review paper by Yazyev[12] deals with the mean-field Hubbard model Hamiltonian calculations on hexagonal, triangular, and bow-tie shaped GNDs. It has been shown that in hydrogen saturated TZGND, $C_{22}H_{12}$, which is a hypothetical PAH molecule called triangulane, the spin polarization lifts the degeneracy of the zero-energy electronic states and opens an energy gap ≈ 0.8 eV.[12] Since these magnetic systems are more reactive than the non-magnetic polyaromatic molecules, there have been few authors who have reported successful synthesis of chemical derivatives of TZGNDs. Although $C_{13}H_9$, the lowest size hydrogen saturated TZGND has not been synthesized as yet, but its nitrogen derivative (cycl[3.3.3]azine) has been synthesized, and its optical absorption spectra has been measured by Leupin and Wirz.[13] Similarly, the next higher sized hydrogen saturated TZGND, triangulane ($C_{22}H_{12}$) has never been isolated, but its chemical derivatives have been successfully synthesized, and their high spin ground state (triplet) has been verified by means of electron spin resonance measurements.[14,15] A large number of theoretical studies of TZGNDs have been performed over the years.[8,16,17]

[5,7,18–27] Honerkamp and co-workers[7] have reported a functional renormalization group treat-

ment of TZGNDs and bow-tie shaped GNDs, modeled using finite-size Hubbard like Hamiltonian with honeycomb lattice structure. Using the plane wave based DFT method, Kawazoe and co-workers[18] have found the total ground state spin of hydrogen saturated TZGND-$(m-1)$ to be $S = \frac{1}{2}(m-1)$, where the zigzag number m takes values $2, 3, ..., 15$. Romanovsky *et al.*[23] have studied the effects of reconstruction of zigzag edges with 5-7 defects, for TZGNDs at the TB level. Manolescu and co-authors.[24] have performed density functional theory based calculations of optical properties of triangular core-shell mixed graphene-boron nitride GNDs. Dong[25] has investigated the influence of external electric field on the electronic structure of TZGNDs at the TB level. Mortensen and collaborators[26] have studied plasmonic modes in TZGNDs using TB model, coupled with random-phase approximation. Recently, Ghaffarian and Ebrahimi[19] calculated the second and third order polarizabilities of TZGNDs using the Hartree-Fock Su-Sheriffer-Heeger (SSH) model. Yoneda *et al.*[20] computed the static third order optical polarizability of trigonal, rhombic and bow-tie GNDs using the hybrid density functional theory. Yamamoto *et al.*[16] have studied the optical absorption of the triangular GNDs with zigzag and armchair edges, using the TB method, within the Hückel approximation. Ezawa[22] has performed calculations on electronic and magnetic properties of TZGNDs, using the TB and Hubbard models. Rossier and Palacios[5] have computed the electronic structure of TZGNDs, using the Hubbard model. Ezawa,[28] as well as, Rossier and Palacios,[5] have argued that for TZGNDs within the Hubbard model, the ground state spin scales linearly with their size. Hawrylak and collaborators[8] have explored the absorption spectra of gated TZGNDs, using the TB, HF and CI methods. Recently, correlated calculations of optical absorption in diamond shaped graphene quantum dots have been performed in our group by Basak *et al.*[27] using Pariser-Parr-Pople (PPP) model.

I. THEORETICAL BACKGROUND

The bipartite lattice of GNDs consists of two mutually interconnected sublattices A and B in which each atom in sublattice A has B as its nearest neighbor, and vice versa. Lieb's theorem predicts the spin state of a half-filled bipartite system, within the Hubbard model with repulsive interactions, to be,[29]

$$S = \frac{1}{2}|N_A - N_B| \tag{1}$$

where N_A and N_B are the numbers of sites in sublattices A and B, with total number of sites $(N_A + N_B)$ as even.

In this work, the ground state calculations have been presented for three sizes of TZGNDs, namely TZGND-n, $n = 1 - 3$, containing 13, 22, and 33 atoms respectively, as shown in Figure 1. C_{2v} point group symmetry has been used for these systems, and only two of the irreducible representations, namely, A_1 and B_2 are relevant, given the planar nature of the systems. It can be understood that the triangular shape of the TZGNDs, results in an unequal number of atoms, N_A and N_B, in the two sublattices, leading to the so called "sublattice imbalance". This, in turn, leads to a total non-zero spin (intrinsic magnetism) for the ground state of the system as per Lieb's theorem (*cf.* equation 1). As seen in the Figure 1, TZGND-1 has $N_A = 7$ and $N_B = 6$, TZGND-2 has $N_A = 12$ and $N_B = 10$, and TZGND-3 has N_A and N_B, as 18 and 15, and TZGND-4 has N_A and N_B as 25 and 21, respectively. The number of atoms in A and B sublattices, N_A and N_B, have been taken to be equal to the majority spins (α) and minority spins (β) respectively. Thus, TZGND-1 has one majority spin more than the minority spin, so that a total spin of $\frac{1}{2}$ is expected, and similarly, TZGND-2, TZGND-3 and TZGND-4 are expected to have total spins of 1, $\frac{3}{2}$ and 2 respectively (*cf.* Figure 1).

As mentioned earlier, Lieb's theorem (*cf.* equation 1) is valid for the Hubbard model with $U > 0$. However, for π-electron systems, it is a well known fact that the inclusion of long-range Coulomb interactions as done in the PPP model is essential for correct description of their electronic structure.[30] Therefore, it is of considerable interest whether the PPP model employed in these calculations, which includes V_{ij} (long range Coulomb interactions), in addition to U, will predict results consistent with the Lieb's theorem. In order to elaborate that we first discuss the case of TZGND-2.

TZGND-2, is a half-filled system with $N = 22$, so that it can have a singlet ground state ($S = 0$), or as per Lieb's theorem, a higher spin, $S = 1$, *i.e.*, triplet as its ground state. Similarly, according to Lieb's theorem, quintet (the higher spin) is the ground state for TZGND-4 ($N = 46$), and the other two lower spin states possible are triplet or singlet. The other two nanodisks, TZGND-1 and TZGND-3, have odd number of electrons, $N = 13$ and $N = 33$ respectively, so that for them, Lieb's theorem is not valid. However, if we assume that the theorem is valid for the odd number of total atoms then, it would predict the ground state as a doublet, $S = \frac{1}{2}$ $(\frac{7-6}{2})$, and a quartet $S = \frac{3}{2}$ $(\frac{18-15}{2})$ for TZGND-1 and

TZGND-3, respectively. However, for the case of TZGND-3, a low spin with $S = \frac{1}{2}$, *i.e.,* a doublet state is also possible. Therefore, these correlated electron calculations have been performed for the doublet spin state for TZGND-1, low and high spin states for TZGND-2 (singlet and triplet), and TZGND-3 (doublet and quartet), and low, intermediate and high spin states for TZGND-4 (singlet, triplet and quintet) respectively.

These calculations were initiated at the UHF level, for the ferromagnetic (FM) states ($S > 0$), as well as for the antiferromagnetic (AFM) state, while for nonmagnetic states, RHF method was employed. Thereafter, the correlated calculations at various levels were performed. FCI calculations have been performed for TZGND-1 (13 atoms), while MRSDCI calculations were done for TZGND-2, TZGND-3 and TZGND-4 because FCI approach is not feasible for them owing to a large number of atoms.

The spin densities at the UHF level are calculated as the difference between the spin up (α) and spin down (β) densities, where the α and β densities are computed from corresponding spin orbitals. The plots of these spin densities help us visualize the magnetic order in the system concerned. Finally, linear absorption spectra of various TZGNDs were calculated, to obtain information about the optical signatures of the spin multiplicities of their ground states. Moreover, the spectra calculated at the PPP model have been compared with those at the TB model level to understand the effect of electron-electron interactions in these disks.

II. RESULTS AND DISCUSSIONS

In this section we examine the evolution of the the spin densities, orbital energy levels with the size of the TZGNDs. We also present the total CI energies corresponding to various spin multiplicities of these disks. Finally, the optical absorption spectra of various TZGNDs are calculated.

A. Nature of frontier orbitals

The energy level diagrams, as functions of eigenstate indices of the nanodisks, have been presented in Figure 2, at TB and UHF levels. In the Figure 2, the screened parameter based

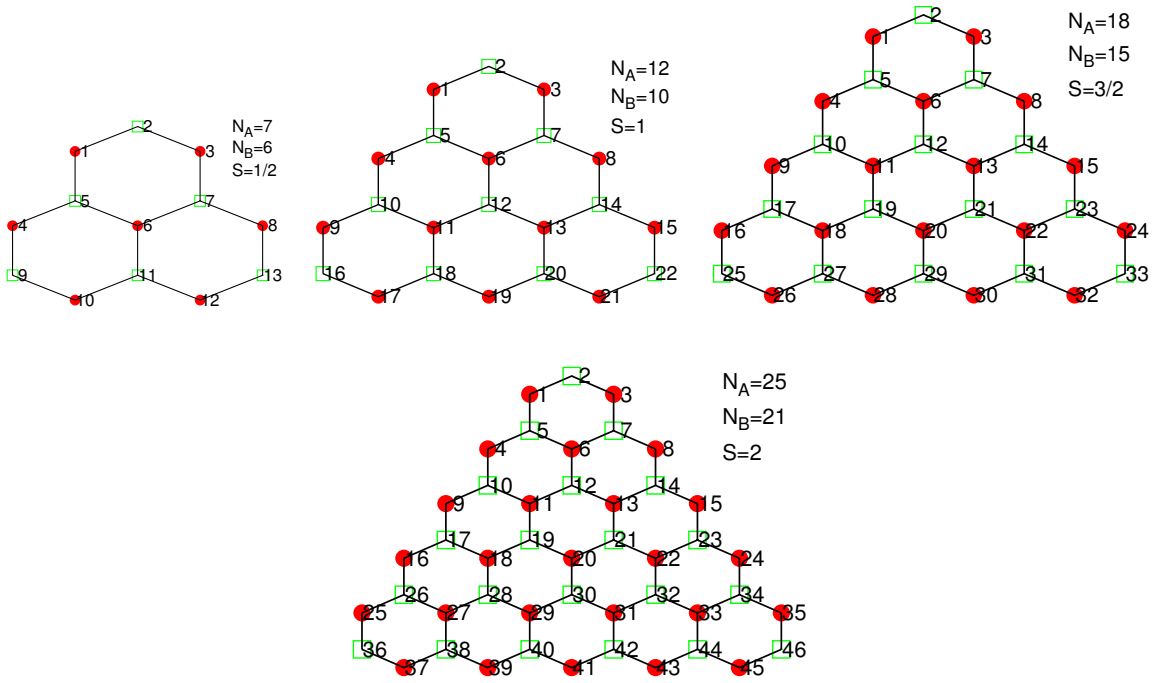

Figure 1: Schematic diagram of trigonal zigzag graphene nanodisks, TZGND-1, 2, 3 and 4 containing 13, 22, 33 and 46 atoms respectively, along with the atom numbering scheme. The total number of atoms in A and B sublattice, N_A (marked as circle) and N_B (marked as square), of the disks and the total spin S, as suggested by Lieb's theorem have been mentioned in the diagram.

calculations have been used for the nanodisks at UHF level, and the energy corresponding to each eigenstate index has been shifted by the chemical potential of the nanodisk (energy associated with the HOMO for the α spin case) in order to simplify the comparison with the TB results. It is evident from the Figure 2, that at TB level, there are one, two, three and four zero energy states (Fermi level degeneracies) for TZGND-n, with n = 1, 2, 3 and 4 respectively,[5,17] while at the UHF level, a partial lifting of degeneracy occurs at the Fermi level. Next, we discuss the nature of frontier orbitals of various TZGNDs in detail.

In Figure 3, the energy level ordering for the important MOs of the TZGNDs contributing to the low-lying excited states have been presented, along with their degeneracies mentioned, at TB and UHF levels. At TB level, for TZGND-1 the singly (highest) occupied MO corresponding to the zero energy states (ZES) is denoted by Z, while for TZGND-2, TZGND-3 and TZGND-4, the MOs corresponding to two, three and four ZES are denoted as Z_1,

Z_2 ; Z_1, Z_2, Z_3; and Z_1, Z_2, Z_3, Z_4 respectively. The states below the HOMOs (ZES) are denoted as $H-1$, $H-2$, and so on, and the states above it, are depicted as $L+1$, $L+2$, ..., for all the nanodisks. At the UHF level, for the cases of both α and β spins, as mentioned earlier, all the energy levels (in units of t) have been shifted by chemical potential of the nanodisk (energy associated with the HOMO for the α spin case), in order to facilitate a direct comparison with the orbital energies at the TB level. It is to be noted that for TZGND-3, the zero energy states (Z_1, Z_2, and Z_3) at the TB model level split into two degenerate states (Z_1, Z_2), and a slightly lower state ($H-1$), whereas for TZGND-4, four ZES (Z_1, Z_2, Z_3 and Z_4) split into two nearly degenerate states (Z and $H-1$), and two degenerate states (($H-2)_1$ and $(H-2)_2$). From the figure 3, it is obvious that similar partial splitting of the degeneracies in other occupied and unoccupied orbitals is seen at the UHF level, as compared to their TB values, for all the TZGNDs. This lifting of the degeneracies is a clear consequence of the influence of electron electron interactions.

B. Spin density distribution

The spin density plots obtained at UHF level by employing the PPP model, for TZGND-1, for both low and high spin states of TZGND-2, TZGND-3, and low, intermediate and high spin states of TZGND-4 are presented in Figure 4. In these calculations, we define the low spin state to be the one which has the minimum possible value of S_z (and not S^2), consistent with the number of electrons in the system, while the high spin state is defined as the one with the S_z value consistent with the Lieb's theorem. The intermediate spin state for the case of TZGND-4 is the one which lies in between the low and the high spin states. It is obvious from the colored figures 4a – 4d that the spin densities alternate between positive (blue-violet) and negative (orange-yellow) values, for the nearest neighbor sites, and hence, we infer that there is an antiferromagnetic order of spins between the adjacent atoms, for TZGND-1, and the high spin states of TZGND-2, TZGND-3 and TZGND-4. While for the low spin states of TGZND-2 and TZGND-3, and for the low and the intermediate spin states of TZGND-4 (*cf.* Figures 4e, 4f, 4g and 4h), this order is broken. As the number of

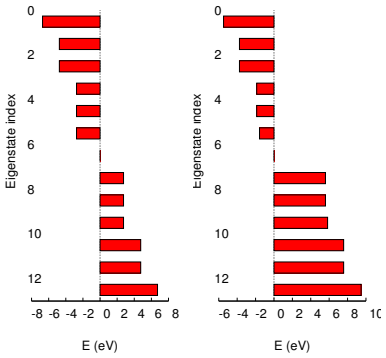

(a) TB (1) (b) UHF (1)

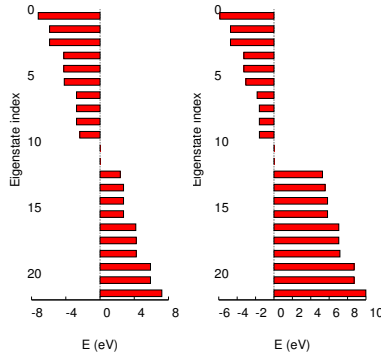

(c) TB (2) (d) UHF (2)

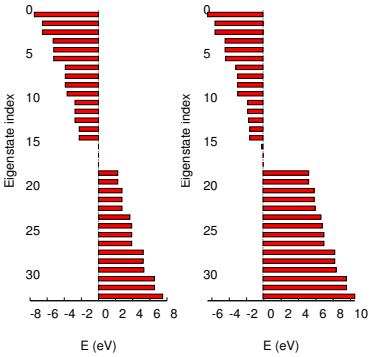

(e) TB (3) (f) UHF(3)

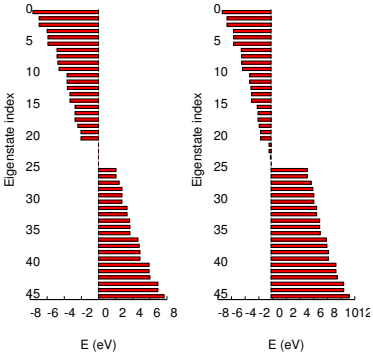

(g) TB (4) (h) UHF(4)

Figure 2: Energy level plots depicting energies (eV) as a function of eigenstate index, (a), (c), (e) and (g) at TB Level and (b), (d), (f) and (h) at UHF level, for TZGND-1, TZGND-2, TZGND-3 and TZGND-4 respectively, using the screened parameters employed in the PPP model Hamiltonian.

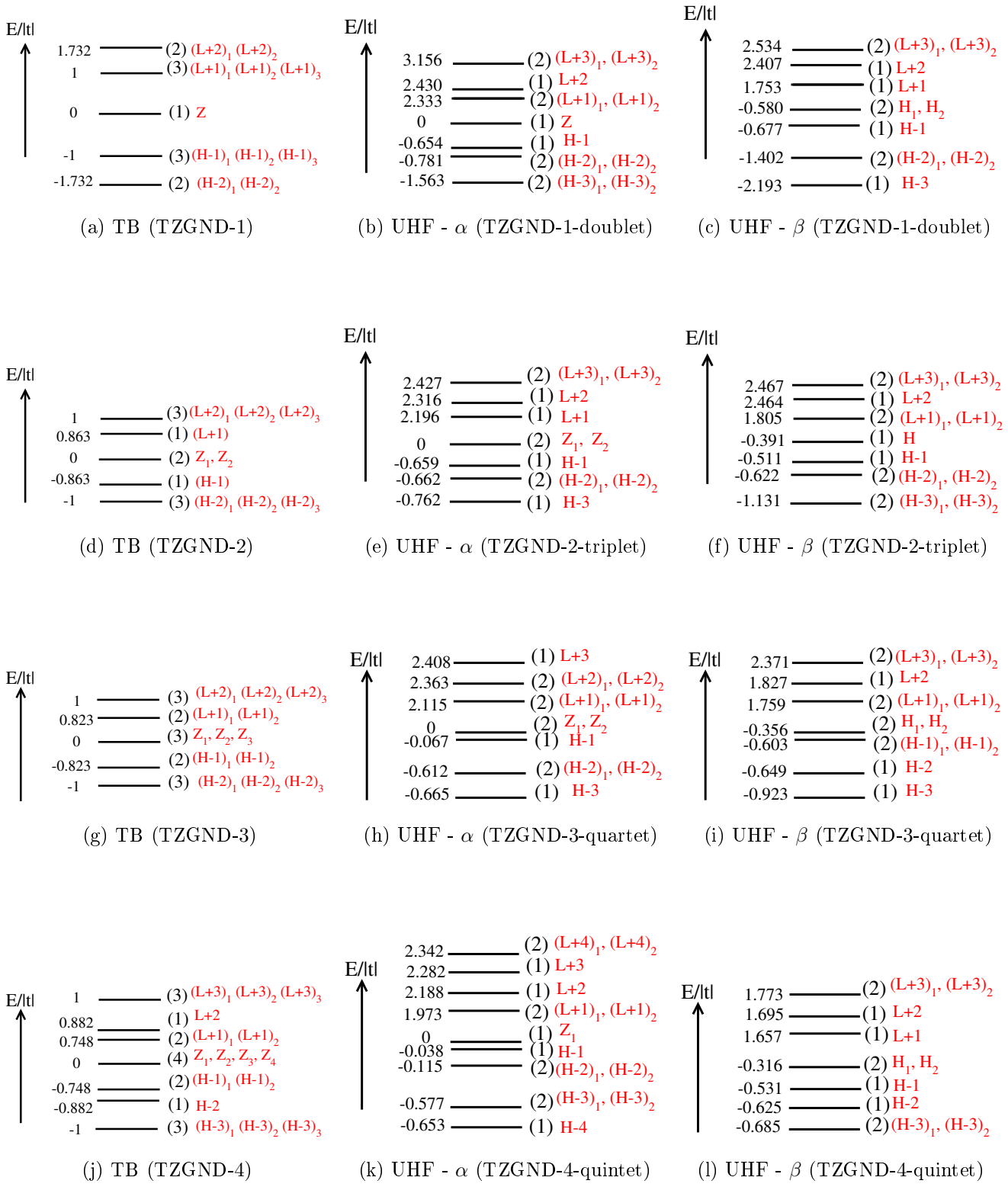

(a) TB (TZGND-1) (b) UHF - α (TZGND-1-doublet) (c) UHF - β (TZGND-1-doublet)

(d) TB (TZGND-2) (e) UHF - α (TZGND-2-triplet) (f) UHF - β (TZGND-2-triplet)

(g) TB (TZGND-3) (h) UHF - α (TZGND-3-quartet) (i) UHF - β (TZGND-3-quartet)

(j) TB (TZGND-4) (k) UHF - α (TZGND-4-quintet) (l) UHF - β (TZGND-4-quintet)

Figure 3: Schematic diagram of the frontier TB and UHF MOs, for TZGND-1 to TZGND-4 with their energies (in units of t) given. At UHF level, the mentioned energies are for the screened parameter calculations. Degeneracies of the MOs are indicated in the brackets next to the energy levels. Energy spacings are not up to the scale.

edge atoms for the TZGND-n is $6(n+1)$, which is an even number, therefore, it is obvious from these figures (4a – 4c), the total edge spin cancels out for TZGND-1, and the high spin states of other nanodisks. Hence, the finite spin, $S = \frac{n}{2}$, is due to the unpaired spins of the internal atoms (*cf.* Figure 4), which increases linearly with the size (n), for these nanodisks. Whereas, in the figures corresponding to the low spin states of TZGND-2, TZGND-3, and the low and the intermediate spin states of TZGND-4 (*cf.* Figures 4e – 4h), as mentioned earlier, the nearest neighbor AFM order is broken in such a manner leading to their lowest possible spins.

C. Spin multiplicity of the ground state

At HF level, the MOs for the high spin states of TZGND-2, TZGND-3 and TZGND-4 possess the required C_{2v} symmetry, while those for the low and the intermediate spins do not. Thus, in order to use the full point group symmetry at the correlated level, the MOs corresponding to the high spin states at the UHF level were employed in all the CI calculations. In Table I, we present the results of our calculations in form of total CI energies, for the lowest states of the two point group ($1A_1$ and $1B_2$), and spin symmetries of TZGNDs.

It is evident from the table, that for TZGND-1, 1^2B_2 is the lowest energy state, irrespective of the choice of Coulomb parameters. For TZGND-2, 1^3B_2 is the lowest energy state, for the high spin state, using both the standard and the screened parameters, while 1^1B_2 is the lowest energy state, for the low spin state, using the standard parameters, and 1^1A_1 is the lowest energy state, for its screened parameters case. Nevertheless, for TZGND-2, it is obvious from the table, that the lowest energy state is 1^3B_2, a result in agreement with Lieb's theorem, even though the PPP model Hamiltonian employed for these calculations includes long range Coulomb interactions. Further, we note that the triplet state is lower than the singlet state (*cf.* Table II) by ≈ 0.5 eV, at the CI level, irrespective of the choice of Coulomb parameters, while the same splitting at the UHF level is found to be ≈ 2 eV. This implies the importance of the electron correlation effects in determining the energetic ordering of the various states of TZGND-2.

For TZGND-3, it is obvious from table I, 1^2B_2 is the lowest state, for the screened parameters, while 1^4A_1 is the lowest one, for the standard parameter case. Thus, the two sets

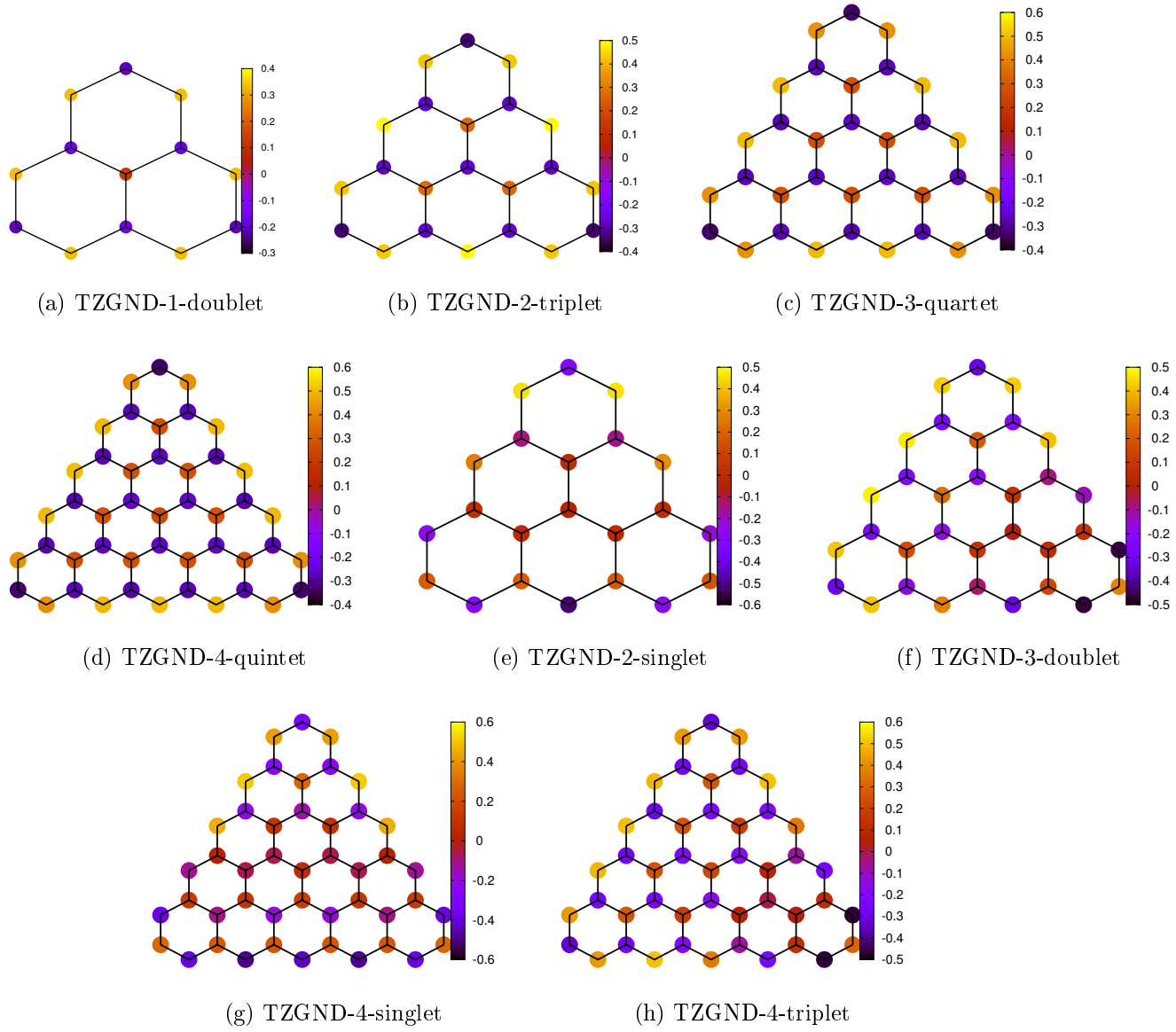

(a) TZGND-1-doublet (b) TZGND-2-triplet (c) TZGND-3-quartet

(d) TZGND-4-quintet (e) TZGND-2-singlet (f) TZGND-3-doublet

(g) TZGND-4-singlet (h) TZGND-4-triplet

Figure 4: (a), (b), (c) and (d) Spin densities of total spin state for TZGND-1 (doublet), for the high spin states of TZGND-2 (triplet), TZGND-3 (quartet), and TZGND-4 (quintet) and those for the low spin states of (e) TZGND-2 (singlet), (f) TZGND-3 (doublet), and the (g) low (singlet) and (h) the intermediate (triplet) spin states of TZGND-4, calculated using the screened parameters, at UHF level within the PPP model Hamiltonian.

of parameters yield contradictory results when it comes to spin multiplicity of the ground state of TZGND-3. However, in majority of cases we have found that the screened parameter based calculations are in better agreement with the experiments, and other theoretical results, as compared to the standard ones.[31–38] Therefore, we are more inclined to trust our

screened parameter based results according to which the low spin state is the ground state for TZGND-3, unlike the case for TZGND-2 for which the higher spin is the ground state. Furthermore, using the screened parameters, the energy splitting (mentioned as *, in Table II) $\approx$ 0.48 eV, with the doublet lower than the quartet. On the other hand, the results obtained using the standard parameters predict the quartet to be lower in energy by a very small amount $\approx$ 0.08 eV, than the doublet state. We also note that UHF calculations performed using both sets of parameters predict the quartet state to be lower than the doublet state by $\approx$ 0.8–0.9 eV. This again implies the importance of the electron correlation effects when it comes to the energetic ordering of the various spin states of TZGND-3. Recently, Krylov *et al.*[39] have reported, using the spin-flip CCSD calculations, that the organic triradical, 5- dehydro-1,3-quinodimethane (5-dehydro-*m*-xylylene, DMX) has electronic ground state of three low-spin coupled unpaired electrons, an "open-shell doublet". However, in our calculations, for the 1^2B_2 state using the screened parameters, we find that the dominant configurations consist of only one electron outside of closed shell, nevertheless, significant contribution also comes from configurations consisting of three open shell electrons coupling to yield a doublet (*cf.* table XLI).

For TZGND-4, the lowest energy state is 1^5A_1, (*cf.* table I) in agreement with Lieb's theorem similar to the case of TZGND-2 containing even number of atoms. This further validates that the PPP model results are consistent with Lieb's theorem (for even number of atoms). Furthermore, we found that the quintet state is lower than the triplet state (*cf.* Table II) by $\approx$ 0.74–0.78 eV, at the CI level, while the same splitting at the UHF level is found to be $\approx$ 0.86–0.9 eV for the standard and the screened parameters respectively. Moreover, the quintet state is below the singlet state by $\approx$ 1.7 eV at the CI level, while the same splitting at the UHF level is found to be $\approx$ 4 eV. Thus, the electron correlation effects are significant for the case of TZGND-4.

Total CI energies (eV)			
		$1A_1$	$1B_2$
TZGND-1 doublet	std	-29.1435	-31.3582
	scr	-25.7362	-27.7212
TZGND-2 singlet (low spin)	std	-53.6842	53.6991
	scr	-47.0545	-46.9789
TZGND-2 triplet (high spin)	std	-51.8313	-54.2466
	scr	-45.4994	-47.5502
TZGND-3 doublet (low spin)	std	-81.6458	-81.6509
	scr	-71.4882	-71.4934
TZGND-3 quartet (high spin)	std	-81.7342	-79.2455
	scr	-71.0065	-68.7229
TZGND-4 singlet (low spin)	std	-112.1262	-112.8375
	scr	-96.9797	-96.9641
TZGND-4 triplet (intermediate spin)	std	-113.9107	-113.0853
	scr	-97.8770	-97.7962
TZGND-4 quintet (high spin)	std	-114.6553	-111.4420
	scr	-98.6637	-96.7086

Table I: Total CI energies (eV), for $1A_1$ and $1B_2$ states, for the various spin states of TZGND-1, TZGND-2, TZGND-3 and TZGND-4, using both the standard (std) and the screened (scr) parameters.

Energy splitting (eV)			
		std	scr
TZGND-2	HF	2.02	1.98
TZGND-2	MRSDCI	0.55	0.50
TZGND-3	HF	0.81	0.91
TZGND-3	MRSDCI	0.08	0.48*
		inter	mediate
TZGND-4	HF	0.86	0.90
TZGND-4	MRSDCI	0.74	0.78
		low	
TZGND-4	HF	4.08	3.89
TZGND-4	MRSDCI	1.82	1.68

Table II: Energy splitting (eV) between the high and the low spin states, of TZGND-2 and TZGND-3, and between the high and the intermediate states (for comparison, the splitting between the high and the low spin is also shown) of TZGND-4, at both HF and MRSDCI level of calculations, using the standard (std) and the screened (scr) parameters. For TZGND-3, screened parameter calculations predict the low spin state to be lower in energy than the high spin state, mentioned by the asterisk symbol (*) in contrast to the TZGND-2 and TZGND-4 calculations.

D. Linear Absorption Spectra at TB and CI levels of calculation

We have computed the absorption spectra for the doublet spin state of TZGND-1, while those for the low and high spin states of TZGND-2 (singlet and triplet), and TZGND-3 (doublet and quartet), and the low, the intermediate and the high spin states of TZGND-4 at TB and CI levels, as shown in Figure 5. While performing these calculations, α (spin up) and β (spin down) are used as the majority and the minority spins respectively.

The absorption spectra obtained at the two levels exhibit the following important features:

- At both levels, the absorption spectrum is red-shifted with increase in size of the TZGNDs.

- There are broadly two main peaks in the spectra of the disks, apart from less intense peaks at higher energies, and the number of peaks increases with increasing size of the disks, at each of the two calculation levels.

- At TB level, the first peak (I) is the most intense peak and the next peak (II) is the second most intensity peak for odd numbered nanodisks namely TZGND-1 and TZGND-3, while for the even numbered nanodisk, TZGND-2, the first peak is the second most intense peak while the second peak contains the highest intensity. For TZGND-4, the first peak (I) is the most intense peak similar to the case of TZGND-1 and TZGND-3. There is an emergence of a small (less intensity) peak (II) and the third peak is the second most intense peak (peak III) for the case of TZGND-4. Whereas at the CI level, the first peak is a low intensity peak for each of the nanodisk, while the most intense peak occurs at a higher energy in TZGNDs. Therefore, this change in the intensity profile in CI can be attributed to electron correlations effects.

- At TB level, the two intense peaks occur at $\approx$ 2.2 eV and 4.5 eV irrespective of the size of the nanodisk while, at CI level the most intense peak occurs $\approx$ 5.5–6.5 eV for TZGND-1, $\approx$ 4–4.25 eV for both low and high spin states of TZGND-2 and TZGND-3, and $\approx$ 3–5 eV for the low, intermediate and high spin states of for TZGND-4, irrespective of the choice of Coulomb parameters.

Next we discuss the specific features of our results at both levels of calculation.

1. One electron calculations

Here, we present and discuss the results of one electron calculations performed using TB model within the PPP model.

At TB level, there exists a very high intensity peak at zero energy (not shown in the figure 2) for TZGND-1, the low spin states of TZGND-2 (singlet) and TZGND-3 (doublet), and the low and the intermediate spin states of TZGND-4 (singlet and triplet), while no such peak is present for their high spin cases (triplet, quartet and quintet respectively). This is

because at TB level, if the total spin is considered to be a good quantum number, then for the case of TZGND-2, the electronic excitations involving Z_1, and Z_2, will be zero energy excitations within the spin singlet space. It is obvious that no such excitation is possible in the triplet manifold, thereby leading to an absence of the zero energy peak for the high spin case. Similar arguments also hold for TZGND-3 and TZGND-4. Therefore, at TB level itself, it is possible to distinguish between the low and high spin states of TZGND-2, TZGND-3 and TZGND-4 (including the intermediate spin state of TZGND-4), by checking their optical absorption spectra for the presence of an intense peak at zero energy. The rest of the peaks are same for the low and high spin cases for these nanodisks at the TB level, and thus, we have presented only the high spin case for each of them. The first peak for all the nanodisks is due to the excitations of the type $Z_i \rightarrow (L+1)_j$, and their respective charge conjugates $(H-1)_j \rightarrow Z_i$, where i and j take values consistent with the degeneracies of the nanodisks. As mentioned earlier, the first peak happens to be the most intense peak for TZGND-1, TZGND-3 and TZGND-4, but for TZGND-2, the second peak involving excitations $Z_i \rightarrow (L+2)_j$, and $(H-2)_j \rightarrow Z_i$, corresponds to its most intense peak. The many-body wave functions of the excited states contributing to the spectra of the nanodisks at TB level have been presented in the Tables III–XXXI in Appendix III.

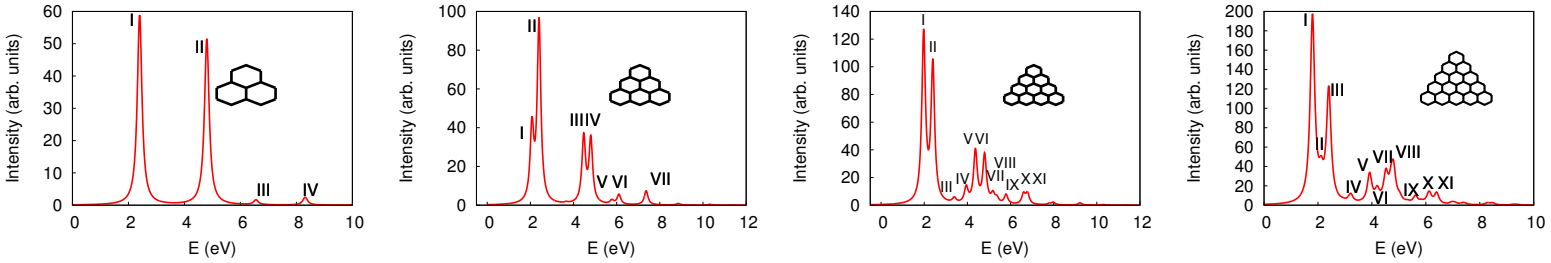

(a) 1 (TB) (b) 2 (TB) (c) 3 (TB) (d) 4 (TB)

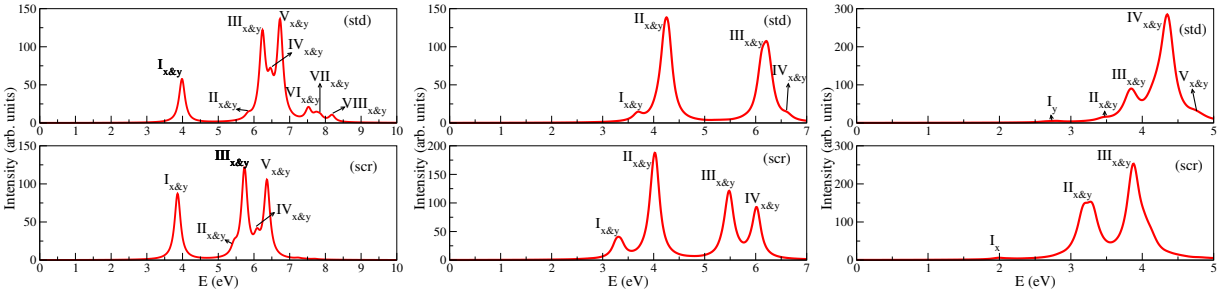

(e) 1-doublet (CI) (f) 2-triplet (CI) (g) 3-quartet (CI)

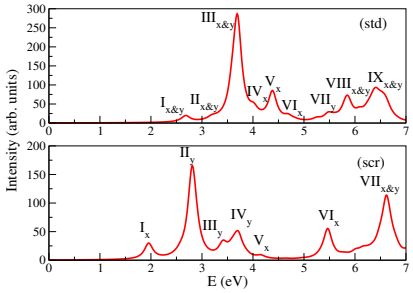

(h) 4-quintet (CI)

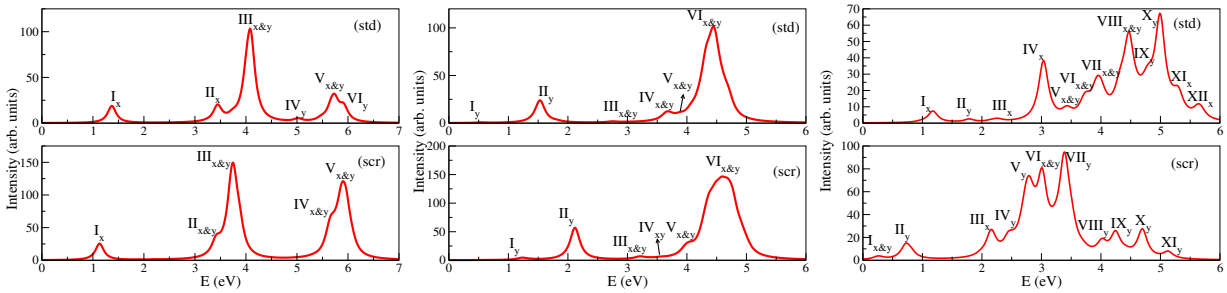

(i) 2-singlet (CI) (j) 3-doublet (CI) (k) 4-triplet (CI)

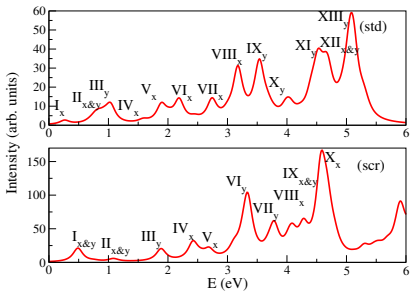

(l) 4-singlet (CI)

Figure 5: Linear absorption spectra of (a) TZGND-1, (b) TZGND-2, (c) TZGND-3, and (d) TZGND-4 at TB, and CI levels. CI calculations were performed using the PPP model. For the TB case, zero energy peaks have been removed. A uniform line width of 0.1 eV was assumed while plotting the spectra.

2. *Correlated electron calculations*

Next, we discuss the nature of the excitations in the optical absorption spectra of various TZGNDs, calculated at the CI level. The many-particle wave functions of the excited states corresponding to the different peaks for the nanodisks at the CI level are summarized in the tables XXXII–XLIX in Appendix III.

For TZGND-1, each peak in the absorption spectra is doubly degenerate, irrespective of the choice of Coulomb parameters, due to the point group symmetry of the system. The first peak is located at ≈ 4 eV, irrespective of the choice of Coulomb parameters, and the dominant configurations contributing to this peak are, $Z \rightarrow (L+1)_i$, and $|(H-2)_i \rightarrow Z\rangle$. The highest intensity peak in the absorption spectra of TZGND-1, has two dominant configurations from the singly excited transitions, $(H-2)_i \rightarrow L+2$, and $H-1 \rightarrow (L+1)_i$, where $i = 1-2$. Although, the nature of the dominant configurations contributing to the most intense peak, calculated using the standard and the screened parameters are identical to each other, yet it is to be noted that the position of this peak calculated using the standard parameter is blue shifted by ≈ 1 eV, from that for the screened parameters case. Remainder of the peaks are discussed in the tables XXXII–XXXIV.

For TZGND-2, for the low spin case, with both the sets of Coulomb parameters, the first peak is located in the range 1.15-1.38 eV, and consists of excitations, $Z_1 \rightarrow Z_2$, and $Z_2 \rightarrow Z_1$, irrespective of the choice of Coulomb parameters. This is identical to the nature of excitations leading to the zero energy peak at the TB level, for the low spin case, discussed in the previous section. Thus, the inclusion of electron correlation effects, blue shifts the zero energy peak to ≈ 1 eV. Furthermore, compared to the TB results where the zero energy peak was the most intense peak, the relative intensity of this peak at the CI level is considerably reduced compared to other peaks in the spectra. Both with standard and screened parameters, the highest intensity peaks are located in the range 3.75–4.06 eV, and one of the configurations which contribute the most to this peak is, $Z_i \rightarrow L+2$. Other dominant configurations which contribute to this peak are parameter dependent, with $Z_1 \rightarrow (L+3)_1$, contributing to the screened parameter wave function, and $H-3 \rightarrow Z_i$, contributing to the standard one (*cf.* Tables XXXV and XXXVI).

For the high spin case of TZGND-2, the first peak is located in the range 3.3–3.7 eV, and the important configurations contributing the most to the peak, are due to excitations, $Z_i \rightarrow L+1$, and $H-1 \rightarrow Z_i$, irrespective of the choice of Coulomb parameters. Although the nature of excitations contributing to this peak are same as those for peak I in the TB level (*cf.* figure 5), in the CI calculations, the peak is blue shifted by $\approx$ 1.3–1.7 eV, along with a reduction in its relative intensity. The location of the most intense peak is in the range 4.02–4.27 eV, which is blue shifted from the TB model result, by $\approx$ 2 eV. In the higher energy regions, for both the spin states, there are peaks at 5.5 eV and 6 eV, except that their relative intensities are reversed, calculated using the screened parameters (*cf.* Tables XXXVII and XXXVIII).

For TZGND-3, for the low spin case, using the standard parameters, the first peak is red shifted by 0.8 eV, from that of the screened parameters, but the dominant contributions to this peak, $Z_2 \rightarrow H-1$, and $H-1 \rightarrow Z_2$, are same in both cases. Since, these excitations involve a zero energy state and the closely spaced state, $H-1$, thus, are similar in nature to the excitations causing the zero energy peak in the TB calculations. The most intense peak is located in the range $\approx$ 4.45–4.60 eV, and consists of several closely spaced states which are a mixture of a number of configurations (*cf.* tables XXXIX–XLI), for both sets of parameters.

For the high spin case of TZGND-3, the location of the first peak is around 2 eV, using the screened parameters, and 2.6 eV using the standard parameters, and the dominant configurations for this peak are, $H-1 \rightarrow (L+1)_1$, $(H-2)_1 \rightarrow H-1$, and $(H-2)_2 \rightarrow H-1$. These excitations are similar to the TB results, as they involve $H-1$ state, which had split from the zero energy states. The most intense peak is located around 3.9–4.35 eV (*cf.* tables. XLII and XLIII), and similar to the case of low spin, several closely spaced states exhibiting strong configuration mixing contribute to it. The configurations contributing to this peak at CI level, are similar to the ones contributing to the corresponding peak in the TB spectrum (*cf*. peak I in Figure 5 and table XII), in the sense that CI excitations involve levels which have split off from the respective degenerate TB levels.

Similar to the low spin case of TZGND-3, the first peak is red-shifted by $\approx$0.23 eV as compared to that in the screened ones, for the low spin case of TZGND-4. The dominant configurations contributing to the peak located in the energy range of 0.25–0.5 eV consist of a mixture of single and double excitations $Z \rightarrow H-1$, and $Z \rightarrow (H-2)_2$; $Z \rightarrow H-1$ using the

standard parameters, and $Z \rightarrow (H-2)_1; Z \rightarrow (H-2)_2$ and $Z \rightarrow (H-2)_2; (H-2)_1 \rightarrow H-1$ using the screened parameters. For the intermediate spin state of TZGND-4, in contrast to its low spin case, using the standard parameters, the first peak is located at 1.2 eV and is blue-shifted by 0.8 eV from that in the screened case, and the most important configurations corresponding to the peak are single excitations, $Z \rightarrow H-1$ (standard parameters) and $(H-2)_2 \rightarrow Z$ and $H-1 \rightarrow Z$ (screened parameters).

For the high spin case of TZGND-4, the first peak is located in the range 1.95–2.70 eV, and the important configurations contributing the most to the peak, are due to single excitations, $Z \rightarrow (L+1)_i$, $H-1 \rightarrow (L+1)_i$, $(H-3)_i \rightarrow Z$ and $(H-3)_i \rightarrow H-1$ (i=1–2), irrespective of the choice of Coulomb parameters. Similar to the case of other nanodisks (TZGND-2 and TGZND-3), these excitations involve a zero energy state and respective split of states, (for TZGND-4, the split states consist of a closely spaced state $H-1$, and two degenerate states $(H-2)_1$ and $(H-2)_2$) correspond to the zero energy excitations in the TB calculations. The location of the most intense peak is in the range 2.8–3.7 eV (*cf.* tables LI–LIII), which is blue shifted from the TB model result, by $\approx$ 1–1.7 eV. Unlike the high spin state case, there exist peaks in the lower energy regions for the low (0.25–0.5 eV) and the intermediate spin states (1.2 eV), and in the higher energy regions, there are intense peaks at $\approx$ 3.5 eV and $\approx$ 5 eV for both the low and the intermediate spin states of TZGND-4 (*cf.* tables XLIV, XLVI, XLVII and XLIX).

We have noted in the preceding discussion, that several peaks observed in CI calculations exhibit similarities to peaks in TB spectrum, in that a common sets of excitations contribute to both. However, in all such cases, the correlated electron peaks were blue shifted compared to TB results, along with significant changes in the intensity profile. It is these distinctions which signify the influence of electron correlations on the optical absorption spectra of these systems.

E. Optical signatures of the spin multiplicities of TZGND-2, TZGND-3 and TZGND-4

In view of the above mentioned features of the absorption spectra at the CI level, it is quite interesting to note that, there exist peaks in the low energy region (1–2 eV), of the low spin state absorption spectra of TZGND-2 and TZGND-3, and also for the low (0.25–0.5 eV)

and intermediate spin states (1.2 eV) of TZGND-4, but not in their high spin state spectra. Therefore, by using optical absorption spectroscopy, one can determine the spin multiplicity of the state from which the absorption is taking place by noticing the presence or absence of these low energy peaks. As per our calculations, the high and low spin states of TZGND-2 and TZGND-3 are energetically well separated ($\approx$ 0.5 eV), and the same for the case of the low and intermediate spin states of TZGND-4. Therefore, an important prediction of our work is that in room temperatures experiments: (a) TZGND-2 should not exhibit any absorption till 3 eV, while (b) TZGND-3 will exhibit lowest absorption feature close to 1 eV, and no absorptions below 2 eV for TZGND-4, based upon our screened parameter results. Thus, it is very interesting to note that optical spectroscopy can be used to probe the magnetic states of these nanodisks.

III. CONCLUSIONS

In this work, we present electronic, magnetic, and optical properties of trigonal zigzag graphene nanodisks of increasing sizes, namely TZGND-1, TZGND-2, TZGND-3 and TZGND-4 containing 13, 22, 33 and 46 atoms respectively, using TB, and large scale CI calculations employing the PPP Hamiltonian. The calculations were performed for various possible spin states of the nanodisks to determine the spin multiplicity of the ground states.

Our calculations show that at TB level, there are one, two, three and four zero energy states for TZGND-1, TZGND-2, TZGND-3 and TZGND-4 respectively, whereas a partial lifting of degeneracies of different occupied and unoccupied states, occurs at the UHF level for these disks. For TZGND-2, the degeneracy of the zero energy states remain intact, while for TZGND-3, with the screened parameter calculations, the degeneracy of the zero energy states is partly broken, but by a relatively small magnitude ($\approx$ 0.067 eV). The upliftment of the degeneracy of the zero energy states is further enhanced in the case of TZGND-4 ($\approx$ 0.115 eV).

It has been found that at UHF level, there occurs an antiferromagnetic order of spins between the nearest atoms of TZGND-1, and the high spin states of other nanodisks, while no such order is present for their low spin states. Hence, for TZGND-1, and the high spin states of other nanodisks, their total edge spins cancel out, and their finite spins are due to

the interior atoms.

The ground state calculations have been performed to check whether the results obtained with the PPP model (which has long-range Coulomb interactions, in addition to the on-site Coulomb repulsion U of the Hubbard model) are consistent with those of Lieb's theorem valid for the Hubbard model. Our calculated total CI energies for various spin multiplicities of the disks predict the high spin state (triplet and quintet) to be lower in energy than the low spin state (singlet, and triplet or singlet) for TZGND-2 and TZGND-4, containing even number of atoms (22 and 46) respectively, and thus, confirming the validity of Lieb's theorem at the PPP model level. For TZGND-3, for which Lieb's theorem is not strictly valid, our calculations predict contradictory results from the two sets of Coulomb parameters. The low spin state (doublet) is found to be lower in energy (≈ 0.48 eV) than the high spin state (quartet), using the screened parameters, while the standard ones predict the energy difference between the two spin states as ≈ 0.08 eV.

The linear absorption spectra of these nanodisks have also been calculated, to obtain information about the optical signatures of the spin multiplicities of their ground states. At TB level, the calculated absorption spectra, for the case of TZGND-2, TZGND-3 and TZGND-4 predict the first peak of very high intensity, located at zero energy. Our absorption calculations performed at CI level are different from those obtained at the TB level as there exists no zero energy peak. Our calculations predict that the first peak has a lesser intensity, and the most intense peak occurs at a higher energy which can be understood as an effect of inclusion of the electron correlations. In this work, we also make a very important prediction for experimentalists which will allow them to detect the spin multiplicities of the ground states of these nanodisks using optical absorption spectroscopy. Based upon our calculations, we predict that at room temperatures, TZGND-2 and TZGND-4 will be optically transparent till 3 eV and 2 eV respectively. As far as TZGND-3 is concerned, because of the contradictory results regarding the ground state multiplicity obtained using the standard and the screened parameters, the presence (absence) of an absorption peak close to 1 eV will confirm the low spin (high spin) nature of the ground state. In an earlier work from our group, the use of electro-absorption spectroscopy was proposed to determine the nature of ground state magnetism in zigzag graphene nanoribbons.[1] The distinctive feature of the present work is that, as per our predictions, the ground state spin multiplicity of TZGNDs can be determined without the use of an external electric field.

WAVE FUNCTION ANALYSIS- TB MODEL

The following tables (III–XXXI) contain the detailed information about the configurations contributing to the peaks in the absorption spectra of TZGNDs at TB level (*cf.* Figure 5).

Table III: Excitation energies as obtained in the linear optical absorption spectrum of TZGND-1, from its doublet spin state, using the TB method. The table contains dominant contributing configurations, excitation energies of the excited states corresponding to the various peaks of the spectrum, dipole matrix elements.

Peak	E (eV)	Transition Dipole (Å)		dominant contributing configurations
		$x-$pol	$y-$pol	
I	2.40	-0.3905	-0.9474	$\|Z \rightarrow (L+1)_1\rangle$
		1.0018	0.0528	$\|Z \rightarrow (L+1)_2\rangle$
		0.5603	-0.7547	$\|Z \rightarrow (L+1)_3\rangle$
		-0.0629	-1.2100	$\|(H-1)_1 \rightarrow Z\rangle$
		0.5949	-0.0683	$\|(H-1)_2 \rightarrow Z\rangle$
		1.0546	-0.0336	$\|(H-1)_3 \rightarrow Z\rangle$
II	4.80	-0.5025	0.1642	$\|(H-1)_1 \rightarrow (L+1)_1\rangle$
		-0.2927	-0.0002	$\|(H-1)_1 \rightarrow (L+1)_2\rangle$
		0.5512	0.0745	$\|(H-1)_1 \rightarrow (L+1)_3\rangle$
		0.5721	-0.3890	$\|(H-1)_2 \rightarrow (L+1)_1\rangle$
		-0.0500	0.2752	$\|(H-1)_2 \rightarrow (L+1)_2\rangle$
		0.5095	0.5235	$\|(H-1)_2 \rightarrow (L+1)_3\rangle$
		-0.1955	-0.1869	$\|(H-1)_3 \rightarrow (L+1)_1\rangle$
		0.0020	-0.8268	$\|(H-1)_3 \rightarrow (L+1)_2\rangle$
		-0.1293	0.1845	$\|(H-1)_3 \rightarrow (L+1)_3\rangle$
III	6.55	0.0059	-0.1023	$\|(H-2)_2 \rightarrow (L+1)_2\rangle$
IV	8.31	0.1632	-0.0631	$\|(H-2)_1 \rightarrow (L+2)_1\rangle$
		0.0631	0.1632	$\|(H-2)_1 \rightarrow (L+2)_2\rangle$
		0.0631	0.1632	$\|(H-2)_2 \rightarrow (L+2)_1\rangle$
		-0.1632	0.0631	$\|(H-2)_2 \rightarrow (L+2)_2\rangle$

Table IV: Excitation energies as obtained in the linear optical absorption spectrum of TZGND-2, from its singlet spin state, using the TB method. The rest of the information is same as that in Table III.

Peak	E (eV)	Transition Dipole (Å)		dominant contributing configurations
		$x-$pol	$y-$pol	
	0.00	-0.3428	1.3574	$\|Z_1 \rightarrow Z_2\rangle$
I	2.07	0.7668	0.5972	$\|H-1 \rightarrow Z_2\rangle$
		0.5972	-0.7668	$\|Z_1 \rightarrow L+1\rangle$
II	2.40	-0.2708	-0.2651	$\|(H-2)_1 \rightarrow Z_2\rangle$
		-0.9057	1.0813	$\|(H-2)_2 \rightarrow Z_2\rangle$
		0.2667	0.3665	$\|(H-2)_3 \rightarrow Z_2\rangle$
		-0.4237	-0.7570	$\|Z_1 \rightarrow (L+2)_1\rangle$
		-0.6903	0.0566	$\|Z_1 \rightarrow (L+2)_2\rangle$
		-0.8472	-0.6234	$\|Z_1 \rightarrow (L+2)_3\rangle$
III	4.47	0.3045	0.5356	$\|(H-2)_1 \rightarrow L+1\rangle$
		-0.0050	0.2516	$\|(H-2)_2 \rightarrow L+1\rangle$
		-0.5792	0.2794	$\|(H-2)_3 \rightarrow L+1\rangle$
		0.2474	0.5781	$\|H-1 \rightarrow (L+2)_1\rangle$
		-0.6056	0.2303	$\|H-1 \rightarrow (L+2)_2\rangle$
		0.0175	-0.2024	$\|H-1 \rightarrow (L+2)_3\rangle$
IV	4.80	0.5676	-0.3866	$\|(H-2)_1 \rightarrow (L+2)_1\rangle$
		-0.2593	-0.3253	$\|(H-2)_1 \rightarrow (L+2)_2\rangle$
		0.1426	0.0075	$\|(H-2)_1 \rightarrow (L+2)_3\rangle$
		-0.1444	-0.0819	$\|(H-2)_2 \rightarrow (L+2)_1\rangle$
		-0.2855	-0.3389	$\|(H-2)_2 \rightarrow (L+2)_2\rangle$
		0.2109	0.0765	$\|(H-2)_2 \rightarrow (L+2)_3\rangle$
		-0.2593	-0.3438	$\|(H-2)_3 \rightarrow (L+2)_1\rangle$
		-0.3565	0.4672	$\|(H-2)_3 \rightarrow (L+2)_2\rangle$
		0.2688	0.3225	$\|(H-2)_3 \rightarrow (L+2)_3\rangle$
V	5.77	-0.0800	-0.1328	$\|(H-4)_1 \rightarrow L+1\rangle$
		-0.1328	0.0800	$\|(H-4)_2 \rightarrow L+1\rangle$
		0.0718	0.1374	$\|H-1 \rightarrow (L+4)_1\rangle$
		0.1374	-0.0718	$\|H-1 \rightarrow (L+4)_2\rangle$

Table V: Excitation energies as obtained in the linear optical absorption spectrum of TZGND-2, from its singlet spin state, using the TB method. The table contains the information corresponding to peaks VI and beyond, in continuation of the Table IV. The rest of the information is same as that in Table III.

Peak	E (eV)	Transition Dipole (Å)		dominant contributing configurations
		$x-$pol	$y-$pol	
VI	6.10	0.1838	-0.1292	$\|(H-4)_1 \rightarrow (L+2)_3\rangle$
		-0.0828	-0.1230	$\|(H-4)_2 \rightarrow (L+2)_1\rangle$
		-0.0768	-0.1582	$\|(H-4)_2 \rightarrow (L+2)_3\rangle$
		0.0807	0.1371	$\|(H-2)_1 \rightarrow (L+4)_2\rangle$
		0.1879	-0.1221	$\|(H-2)_2 \rightarrow (L+4)_1\rangle$
		-0.0575	-0.1557	$\|(H-2)_2 \rightarrow (L+4)_2\rangle$
VI	7.36	0.1519	0.2523	$\|(H-4)_1 \rightarrow L+3\rangle$
		0.2523	-0.1519	$\|(H-4)_2 \rightarrow L+3\rangle$
		0.1364	0.2610	$\|H-3 \rightarrow (L+4)_1\rangle$
		0.2610	-0.1364	$\|H-3 \rightarrow (L+4)_2\rangle$

Table VI: Excitation energies as obtained in the linear optical absorption spectrum of TZGND-2, from its triplet spin state, using the TB method. The rest of the information is same as that in Table III.

Peak	E (eV)	Transition Dipole (Å)		dominant contributing configurations
		$x-$pol	$y-$pol	
I	2.07	0.6790	0.6954	$\|Z_1 \rightarrow L+1\rangle$
		-0.6954	0.6790	$\|Z_2 \rightarrow L+1\rangle$
		0.6790	0.6954	$\|H-1 \rightarrow Z_1\rangle$
		-0.6954	0.6790	$\|H-1 \rightarrow Z_2\rangle$
II	2.40	0.3176	0.4037	$\|Z_1 \rightarrow (L+2)_1\rangle$
		-1.0046	0.9878	$\|Z_1 \rightarrow (L+2)_2\rangle$
		0.2813	0.1036	$\|Z_1 \rightarrow (L+2)_3\rangle$
		0.6840	-0.0305	$\|Z_2 \rightarrow (L+2)_1\rangle$
		-0.7253	-0.7499	$\|Z_2 \rightarrow (L+2)_2\rangle$
		-0.3943	-0.7912	$\|Z_2 \rightarrow (L+2)_3\rangle$
		0.0061	0.7034	$\|(H-2)_1 \rightarrow Z_1\rangle$
		0.3815	-0.3358	$\|(H-2)_1 \rightarrow Z_2\rangle$
		0.6600	-0.2671	$\|(H-2)_2 \rightarrow Z_1\rangle$
		-0.0543	-0.4420	$\|(H-2)_2 \rightarrow Z_2\rangle$
		-0.8681	0.7637	$\|(H-2)_3 \rightarrow Z_1\rangle$
		-1.0004	-0.9387	$\|(H-2)_3 \rightarrow Z_2\rangle$
III	4.47	-0.5675	0.3042	$\|(H-2)_1 \rightarrow L+1\rangle$
		-0.3193	-0.5660	$\|(H-2)_2 \rightarrow L+1\rangle$
		0.0650	-0.1238	$\|(H-2)_3 \rightarrow L+1\rangle$
		-0.5711	0.3029	$\|H-1 \rightarrow (L+2)_1\rangle$
		-0.0006	0.2070	$\|H-1 \rightarrow (L+2)_2\rangle$
		-0.3194	-0.5419	$\|H-1 \rightarrow (L+2)_3\rangle$
IV	4.80	-0.4552	0.2968	$\|(H-2)_1 \rightarrow (L+2)_1\rangle$
		-0.3096	-0.3395	$\|(H-2)_1 \rightarrow (L+2)_2\rangle$
		0.2811	0.3506	$\|(H-2)_1 \rightarrow (L+2)_3\rangle$
		0.2713	0.5185	$\|(H-2)_2 \rightarrow (L+2)_1\rangle$
		0.1825	0.0086	$\|(H-2)_2 \rightarrow (L+2)_2\rangle$
		0.5068	-0.2918	$\|(H-2)_2 \rightarrow (L+2)_3\rangle$
		-0.0325	-0.2713	$\|(H-2)_3 \rightarrow (L+2)_1\rangle$
		0.2752	-0.2556	$\|(H-2)_3 \rightarrow (L+2)_3\rangle$

Table VII: Excitation energies as obtained in the linear optical absorption spectrum of TZGND-2, from its triplet spin state, using the TB method. The table contains the information corresponding to peaks V and beyond, in continuation of the Table VI. The rest of the information is same as that in Table III.

Peak	E (eV)	Transition Dipole (Å)		dominant contributing configurations
		$x-$pol	$y-$pol	
V	5.77	-0.0777	-0.1342	$\|(H-4)_1 \rightarrow L+1\rangle$
		0.1342	-0.0777	$\|(H-4)_2 \rightarrow L+1\rangle$
		0.1367	-0.0731	$\|H-1 \rightarrow (L+4)_1\rangle$
		0.0731	0.1367	$\|H-1 \rightarrow (L+4)_2\rangle$
VI	6.10	-0.1872	0.1256	$\|(H-4)_1 \rightarrow (L+2)_2\rangle$
		-0.0741	-0.1576	$\|(H-4)_2 \rightarrow (L+2)_2\rangle$
		-0.0733	-0.1287	$\|(H-4)_2 \rightarrow (L+2)_3\rangle$
		-0.1005	0.0617	$\|(H-2)_2 \rightarrow (L+4)_2\rangle$
		-0.1168	-0.1811	$\|(H-2)_3 \rightarrow (L+4)_1\rangle$
		0.1808	-0.0767	$\|(H-2)_3 \rightarrow (L+4)_2\rangle$
VI	7.36	0.1476	0.2548	$\|(H-4)_1 \rightarrow L+3\rangle$
		-0.2548	0.1476	$\|(H-4)_2 \rightarrow L+3\rangle$
		-0.2597	0.1388	$\|H-3 \rightarrow (L+4)_1\rangle$
		-0.1388	-0.2597	$\|H-3 \rightarrow (L+4)_2\rangle$

Table VIII: Excitation energies as obtained in the linear optical absorption spectrum of TZGND-3, from its doublet spin state, using the TB method. The rest of the information is same as that in Table III.

Peak	E (eV)	Transition Dipole (Å)		dominant contributing configurations
		$x-$pol	$y-$pol	
	0.00	-0.7874	1.3115	$\|Z_1 \rightarrow Z_3\rangle$
		1.2595	-1.7138	$\|Z_2 \rightarrow Z_3\rangle$
		-0.9740	-0.5563	$\|Z_1 \rightarrow Z_2\rangle$
I	1.97	0.0572	1.2328	$\|(H-1)_1 \rightarrow Z_3\rangle$
		1.2328	-0.0572	$\|(H-1)_2 \rightarrow Z_3\rangle$
		-0.6707	0.0652	$\|(H-1)_1 \rightarrow Z_2\rangle$
		0.0652	0.6707	$\|(H-1)_2 \rightarrow Z_2\rangle$
		0.0551	1.0340	$\|Z_1 \rightarrow (L+1)_1\rangle$
		1.0340	-0.0551	$\|Z_1 \rightarrow (L+1)_2\rangle$
		0.0841	0.6686	$\|Z_2 \rightarrow (L+1)_1\rangle$
		0.6686	-0.0841	$\|Z_2 \rightarrow (L+1)_2\rangle$
II	2.40	-0.1666	0.4436	$\|(H-2)_1 \rightarrow Z_3\rangle$
		0.3136	-0.1640	$\|(H-2)_2 \rightarrow Z_3\rangle$
		0.6393	0.5043	$\|(H-2)_3 \rightarrow Z_3\rangle$
		-1.0026	-0.3444	$\|(H-2)_1 \rightarrow Z_2\rangle$
		0.7008	0.3896	$\|(H-2)_2 \rightarrow Z_2\rangle$
		0.2328	-0.7379	$\|(H-2)_3 \rightarrow Z_2\rangle$
		-0.3396	0.2646	$\|Z_1 \rightarrow (L+2)_1\rangle$
		-0.4217	0.7427	$\|Z_1 \rightarrow (L+2)_2\rangle$
		-0.3196	0.7524	$\|Z_1 \rightarrow (L+2)_3\rangle$
		0.8399	0.5945	$\|Z_2 \rightarrow (L+2)_1\rangle$
		0.6162	-0.5408	$\|Z_2 \rightarrow (L+2)_2\rangle$
		-0.6822	-0.4112	$\|Z_2 \rightarrow (L+2)_3\rangle$
		-0.3396	0.2646	$\|Z_1 \rightarrow (L+2)_1\rangle$
		-0.4217	0.7427	$\|Z_1 \rightarrow (L+2)_2\rangle$
		-0.3196	0.7524	$\|Z_1 \rightarrow (L+2)_3\rangle$

Table IX: Excitation energies as obtained in the linear optical absorption spectrum of TZGND-3, from its doublet spin state, using the TB method. The table contains the information corresponding to peaks III and beyond, in continuation of the Table VIII. The rest of the information is same as that in Table III.

Peak	E (eV)	Transition Dipole (Å)		dominant contributing configurations
		$x-$pol	$y-$pol	
III	3.39	-0.0361	-0.2056	$\|(H-4)_1 \rightarrow Z_3\rangle$
		0.1244	-0.0423	$\|(H-4)_2 \rightarrow Z_3\rangle$
		-0.1657	0.0131	$\|(H-4)_3 \rightarrow Z_3\rangle$
		0.1111	-0.0254	$\|(H-4)_1 \rightarrow Z_2\rangle$
		0.0068	0.1449	$\|Z_1 \rightarrow (L+4)_1\rangle$
		-0.1763	0.0040	$\|Z_1 \rightarrow (L+4)_2\rangle$
		0.0028	-0.1007	$\|Z_1 \rightarrow (L+4)_3\rangle$
		-0.1143	0.0109	$\|Z_2 \rightarrow (L+4)_2\rangle$
IV	3.94	0.1753	0.3314	$\|(H-1)_1 \rightarrow (L+1)_1\rangle$
		0.3314	-0.1753	$\|(H-1)_1 \rightarrow (L+1)_2\rangle$
		0.3314	-0.1753	$\|(H-1)_2 \rightarrow (L+1)_1\rangle$
		-0.1753	-0.3314	$\|(H-1)_2 \rightarrow (L+1)_2\rangle$
V	4.37	0.0827	-0.4598	$\|(H-2)_1 \rightarrow (L+1)_1\rangle$
		-0.1505	-0.2631	$\|(H-2)_1 \rightarrow (L+1)_2\rangle$
		0.4913	-0.2869	$\|(H-2)_2 \rightarrow (L+1)_2\rangle$
		-0.4333	-0.2600	$\|(H-2)_3 \rightarrow (L+1)_1\rangle$
		0.1260	0.2082	$\|(H-2)_3 \rightarrow (L+1)_2\rangle$
		-0.0930	-0.1816	$\|(H-1)_1 \rightarrow (L+2)_1\rangle$
		-0.1782	-0.2792	$\|(H-1)_1 \rightarrow (L+2)_2\rangle$
		0.4849	-0.2971	$\|(H-1)_1 \rightarrow (L+2)_3\rangle$
		0.0832	0.5189	$\|(H-1)_2 \rightarrow (L+2)_1\rangle$
		-0.4383	-0.0776	$\|(H-1)_2 \rightarrow (L+2)_2\rangle$

Table X: Excitation energies as obtained in the linear optical absorption spectrum of TZGND-3, from its doublet spin state, using the TB method. The table contains the information corresponding to peaks VI and beyond, in continuation of the Table IX. The rest of the information is same as that in Table III.

Peak	E (eV)	Transition Dipole (Å)		dominant contributing configurations
		$x-$pol	$y-$pol	
VI	4.80	-0.1166	0.5063	$\|(H-2)_1 \rightarrow (L+2)_1\rangle$
		0.2605	-0.0935	$\|(H-2)_1 \rightarrow (L+2)_2\rangle$
		0.2214	0.3540	$\|(H-2)_1 \rightarrow (L+2)_3\rangle$
		0.1386	0.2208	$\|(H-2)_2 \rightarrow (L+2)_1\rangle$
		0.2073	0.4191	$\|(H-2)_2 \rightarrow (L+2)_2\rangle$
		0.5413	-0.2859	$\|(H-2)_2 \rightarrow (L+2)_3\rangle$
		-0.4688	0.1922	$\|(H-2)_3 \rightarrow (L+2)_1\rangle$
		0.3832	0.2375	$\|(H-2)_3 \rightarrow (L+2)_2\rangle$
		-0.1435	-0.2881	$\|(H-2)_3 \rightarrow (L+2)_3\rangle$
VII	5.18	-0.1423	-0.2441	$\|H-3 \rightarrow (L+1)_1\rangle$
		0.2441	-0.1423	$\|H-3 \rightarrow (L+1)_2\rangle$
		0.2399	-0.1492	$\|(H-1)_1 \rightarrow L+3\rangle$
		0.1492	0.2399	$\|(H-1)_2 \rightarrow L+3\rangle$
VIII	5.36	-0.1434	0.0834	$\|(H-4)_2 \rightarrow (L+1)_1\rangle$
		-0.0844	-0.1443	$\|(H-4)_2 \rightarrow (L+1)_2\rangle$
		-0.1136	0.0663	$\|(H-4)_3 \rightarrow (L+1)_1\rangle$
		-0.0654	-0.1121	$\|(H-4)_3 \rightarrow (L+1)_2\rangle$
		-0.0637	-0.1024	$\|(H-1)_1 \rightarrow (L+4)_1\rangle$
		-0.0927	-0.1493	$\|(H-1)_1 \rightarrow (L+4)_3\rangle$
		0.1039	-0.0645	$\|(H-1)_2 \rightarrow (L+4)_1\rangle$
		0.1481	-0.0922	$\|(H-1)_2 \rightarrow (L+4)_3\rangle$

Table XI: Excitation energies as obtained in the linear optical absorption spectrum of TZGND-3, from its doublet spin state, using the TB method. The table contains the information corresponding to peaks IX and beyond, in continuation of the Table X. The rest of the information is same as that in Table III.

Peak	E (eV)	Transition Dipole (Å)		dominant contributing configurations
		$x-$pol	$y-$pol	
IX	5.79	-0.1584	-0.1340	$\|(H-4)_2 \rightarrow (L+2)_1\rangle$
		-0.0673	0.1399	$\|(H-4)_2 \rightarrow (L+2)_2\rangle$
		0.0790	0.1098	$\|(H-4)_2 \rightarrow (L+2)_3\rangle$
		-0.1652	0.0985	$\|(H-2)_1 \rightarrow (L+4)_1\rangle$
		0.0491	0.1009	$\|(H-2)_1 \rightarrow (L+4)_3\rangle$
		-0.1438	0.0792	$\|(H-2)_2 \rightarrow (L+4)_2\rangle$
		-0.1745	-0.0559	$\|(H-2)_2 \rightarrow (L+4)_3\rangle$
		0.1082	-0.0564	$\|(H-2)_3 \rightarrow (L+4)_2\rangle$
		0.0629	0.1230	$\|(H-2)_3 \rightarrow (L+4)_3\rangle$
X	6.60	0.2687	-0.1228	$\|(H-4)_1 \rightarrow L+3\rangle$
		-0.0504	-0.1790	$\|(H-4)_2 \rightarrow L+3\rangle$
		0.1177	0.2037	$\|(H-4)_3 \rightarrow L+3\rangle$
		0.1245	0.2106	$\|H-3 \rightarrow (L+4)_1\rangle$
		0.2523	-0.1576	$\|H-3 \rightarrow (L+4)_2\rangle$
		-0.0971	-0.1393	$\|H-3 \rightarrow (L+4)_3\rangle$
XI	6.78	-0.1723	-0.2477	$\|(H-4)_1 \rightarrow (L+4)_1\rangle$
		0.2415	-0.1466	$\|(H-4)_1 \rightarrow (L+4)_2\rangle$
		0.1316	-0.1293	$\|(H-4)_2 \rightarrow (L+4)_1\rangle$
		-0.1847	0.1131	$\|(H-4)_2 \rightarrow (L+4)_3\rangle$
		-0.1426	-0.2643	$\|(H-4)_3 \rightarrow (L+4)_2\rangle$
		0.1502	-0.0699	$\|(H-4)_3 \rightarrow (L+4)_3\rangle$

Table XII: Excitation energies as obtained in the linear optical absorption spectrum of TZGND-3, from its quartet spin state, using the TB method. The rest of the information is same as that in Table III.

Peak	E (eV)	Transition Dipole (Å)		dominant contributing configurations
		$x-$pol	$y-$pol	
I	1.97	0.0551	1.0340	$\|Z_1 \rightarrow (L+1)_1\rangle$
		1.0340	-0.0551	$\|Z_1 \rightarrow (L+1)_2\rangle$
		0.0841	0.6686	$\|Z_2 \rightarrow (L+1)_1\rangle$
		0.6686	-0.0841	$\|Z_2 \rightarrow (L+1)_2\rangle$
		1.2307	-0.0920	$\|Z_3 \rightarrow (L+1)_1\rangle$
		-0.0920	-1.2307	$\|Z_3 \rightarrow (L+1)_2\rangle$
		0.0551	1.0340	$\|(H-1)_1 \rightarrow Z_1\rangle$
		1.0340	-0.0551	$\|(H-1)_1 \rightarrow Z_2\rangle$
		0.0841	0.6686	$\|(H-1)_1 \rightarrow Z_3\rangle$
		0.6686	-0.0841	$\|(H-1)_2 \rightarrow Z_1\rangle$
		1.2307	-0.0920	$\|(H-1)_2 \rightarrow Z_2\rangle$
		-0.0920	-1.2307	$\|(H-1)_2 \rightarrow Z_3\rangle$
II	2.40	-0.3396	0.2646	$\|Z_1 \rightarrow (L+2)_1\rangle$
		-0.4217	0.7427	$\|Z_1 \rightarrow (L+2)_2\rangle$
		-0.3196	0.7524	$\|Z_1 \rightarrow (L+2)_3\rangle$
		0.8399	0.5945	$\|Z_2 \rightarrow (L+2)_1\rangle$
		0.6162	-0.5408	$\|Z_2 \rightarrow (L+2)_2\rangle$
		-0.6822	-0.4112	$\|Z_2 \rightarrow (L+2)_3\rangle$
		-0.0862	-0.5997	$\|Z_3 \rightarrow (L+2)_1\rangle$
		0.6658	0.2952	$\|Z_3 \rightarrow (L+2)_2\rangle$
		-0.2898	0.1767	$\|Z_3 \rightarrow (L+2)_3\rangle$
		-0.3396	0.2646	$\|(H-2)_1 \rightarrow Z_1\rangle$
		-0.4217	0.7427	$\|(H-2)_1 \rightarrow Z_2\rangle$
		-0.3196	0.7524	$\|(H-2)_1 \rightarrow Z_3\rangle$
		0.8399	0.5945	$\|(H-2)_2 \rightarrow Z_1\rangle$
		0.6162	-0.5408	$\|(H-2)_2 \rightarrow Z_2\rangle$
		-0.6822	-0.4112	$\|(H-2)_2 \rightarrow Z_3\rangle$
		-0.0862	-0.5997	$\|(H-2)_3 \rightarrow Z_1\rangle$
		0.6658	0.2952	$\|(H-2)_3 \rightarrow Z_2\rangle$
		-0.2898	0.1767	$\|(H-2)_3 \rightarrow Z_3\rangle$

Table XIII: Excitation energies as obtained in the linear optical absorption spectrum of TZGND-3, from its quartet spin state, using the TB method. The table contains the information corresponding to peaks III and beyond, in continuation of the Table XII. The rest of the information is same as that in Table III.

Peak	E (eV)	Transition Dipole (Å)		dominant contributing configurations
		$x-$pol	$y-$pol	
III	3.39	0.0068	0.1449	$\|Z_1 \rightarrow (L+4)_1\rangle$
		-0.1763	0.0040	$\|Z_1 \rightarrow (L+4)_2\rangle$
		0.0028	-0.1007	$\|Z_1 \rightarrow (L+4)_3\rangle$
		-0.1143	0.0109	$\|Z_2 \rightarrow (L+4)_2\rangle$
		0.1725	-0.0118	$\|Z_3 \rightarrow (L+4)_1\rangle$
		0.0093	0.2100	$\|Z_3 \rightarrow (L+4)_2\rangle$
		-0.1200	-0.0007	$\|Z_3 \rightarrow (L+4)_3\rangle$
		0.0068	0.1449	$\|(H-4)_1 \rightarrow Z_1\rangle$
		-0.1763	0.0040	$\|(H-4)_1 \rightarrow Z_2\rangle$
		0.0028	-0.1007	$\|(H-4)_1 \rightarrow Z_3\rangle$
		-0.1143	0.0109	$\|(H-4)_2 \rightarrow Z_1\rangle$
		0.1725	-0.0118	$\|(H-4)_2 \rightarrow Z_3\rangle$
		0.0093	0.2100	$\|(H-4)_3 \rightarrow Z_1\rangle$
		-0.1200	-0.0007	$\|(H-4)_3 \rightarrow Z_3\rangle$
IV	3.94	0.1753	0.3314	$\|(H-1)_1 \rightarrow (L+1)_1\rangle$
		0.3314	-0.1753	$\|(H-1)_1 \rightarrow (L+1)_2\rangle$
		0.3314	-0.1753	$\|(H-1)_2 \rightarrow (L+1)_1\rangle$
		-0.1753	-0.3314	$\|(H-1)_2 \rightarrow (L+1)_2\rangle$

Table XIV: Excitation energies as obtained in the linear optical absorption spectrum of TZGND-3, from its quartet spin state, using the TB method. The table contains the information corresponding to peaks V and beyond, in continuation of the Table XIII. The rest of the information is same as that in Table III.

Peak	E (eV)	Transition Dipole (Å)		dominant contributing configurations
		$x-$pol	$y-$pol	
V	4.37	0.0827	-0.4598	$\|(H-2)_1 \rightarrow (L+1)_1\rangle$
		-0.1505	-0.2631	$\|(H-2)_1 \rightarrow (L+1)_2\rangle$
		0.4913	-0.2869	$\|(H-2)_2 \rightarrow (L+1)_2\rangle$
		-0.4333	-0.2600	$\|(H-2)_3 \rightarrow (L+1)_1\rangle$
		0.1260	0.2082	$\|(H-2)_3 \rightarrow (L+1)_2\rangle$
		-0.0930	-0.1816	$\|(H-1)_1 \rightarrow (L+2)_1\rangle$
		-0.1782	-0.2792	$\|(H-1)_1 \rightarrow (L+2)_2\rangle$
		0.4849	-0.2971	$\|(H-1)_1 \rightarrow (L+2)_3\rangle$
		0.0832	0.5189	$\|(H-1)_2 \rightarrow (L+2)_1\rangle$
		-0.4383	-0.0776	$\|(H-1)_2 \rightarrow (L+2)_2\rangle$
VI	4.80	-0.1166	0.5063	$\|(H-2)_1 \rightarrow (L+2)_1\rangle$
		0.2605	-0.0935	$\|(H-2)_1 \rightarrow (L+2)_2\rangle$
		0.2214	0.3540	$\|(H-2)_1 \rightarrow (L+2)_3\rangle$
		0.1386	0.2208	$\|(H-2)_2 \rightarrow (L+2)_1\rangle$
		0.2073	0.4191	$\|(H-2)_2 \rightarrow (L+2)_2\rangle$
		0.5413	-0.2859	$\|(H-2)_2 \rightarrow (L+2)_3\rangle$
		-0.4688	0.1922	$\|(H-2)_3 \rightarrow (L+2)_1\rangle$
		0.3832	0.2375	$\|(H-2)_3 \rightarrow (L+2)_2\rangle$
		-0.1435	-0.2881	$\|(H-2)_3 \rightarrow (L+2)_3\rangle$
VII	5.18	-0.1423	-0.2441	$\|H-3 \rightarrow (L+1)_1\rangle$
		0.2441	-0.1423	$\|H-3 \rightarrow (L+1)_2\rangle$
		0.2399	-0.1492	$\|(H-1)_1 \rightarrow L+3\rangle$
		0.1492	0.2399	$\|(H-1)_2 \rightarrow L+3\rangle$

Table XV: Excitation energies as obtained in the linear optical absorption spectrum of TZGND-3, from its quartet spin state, using the TB method. The table contains the information corresponding to peaks VIII and beyond, in continuation of the Table XIV. The rest of the information is same as that in Table III.

Peak	E (eV)	Transition Dipole (Å)		dominant contributing configurations
		$x-$pol	$y-$pol	
VIII	5.36	-0.1434	0.0834	$\|(H-4)_2 \rightarrow (L+1)_1\rangle$
		-0.0844	-0.1443	$\|(H-4)_2 \rightarrow (L+1)_2\rangle$
		-0.1136	0.0663	$\|(H-4)_3 \rightarrow (L+1)_1\rangle$
		-0.0654	-0.1121	$\|(H-4)_3 \rightarrow (L+1)_2\rangle$
		-0.0637	-0.1024	$\|(H-1)_1 \rightarrow (L+4)_1\rangle$
		-0.0927	-0.1493	$\|(H-1)_1 \rightarrow (L+4)_3\rangle$
		0.1039	-0.0645	$\|(H-1)_2 \rightarrow (L+4)_1\rangle$
		0.1481	-0.0922	$\|(H-1)_2 \rightarrow (L+4)_3\rangle$
IX	5.79	-0.1584	-0.1340	$\|(H-4)_2 \rightarrow (L+2)_1\rangle$
		-0.0673	0.1399	$\|(H-4)_2 \rightarrow (L+2)_2\rangle$
		0.0790	0.1098	$\|(H-4)_2 \rightarrow (L+2)_3\rangle$
		-0.1652	0.0985	$\|(H-2)_1 \rightarrow (L+4)_1\rangle$
		0.0491	0.1009	$\|(H-2)_1 \rightarrow (L+4)_3\rangle$
		-0.1438	0.0792	$\|(H-2)_2 \rightarrow (L+4)_2\rangle$
		-0.1745	-0.0559	$\|(H-2)_2 \rightarrow (L+4)_3\rangle$
		0.1082	-0.0564	$\|(H-2)_3 \rightarrow (L+4)_2\rangle$
		0.0629	0.1230	$\|(H-2)_3 \rightarrow (L+4)_3\rangle$
X	6.60	0.2687	-0.1228	$\|(H-4)_1 \rightarrow L+3\rangle$
		-0.0504	-0.1790	$\|(H-4)_2 \rightarrow L+3\rangle$
		0.1177	0.2037	$\|(H-4)_3 \rightarrow L+3\rangle$
		0.1245	0.2106	$\|H-3 \rightarrow (L+4)_1\rangle$
		0.2523	-0.1576	$\|H-3 \rightarrow (L+4)_2\rangle$
		-0.0971	-0.1393	$\|H-3 \rightarrow (L+4)_3\rangle$
XI	6.78	-0.1723	-0.2477	$\|(H-4)_1 \rightarrow (L+4)_1\rangle$
		0.2415	-0.1466	$\|(H-4)_1 \rightarrow (L+4)_2\rangle$
		0.1316	-0.1293	$\|(H-4)_2 \rightarrow (L+4)_1\rangle$
		-0.1847	0.1131	$\|(H-4)_2 \rightarrow (L+4)_3\rangle$
		-0.1426	-0.2643	$\|(H-4)_3 \rightarrow (L+4)_2\rangle$
		0.1502	-0.0699	$\|(H-4)_3 \rightarrow (L+4)_3\rangle$

Table XVI: Excitation energies as obtained in the linear optical absorption spectrum of TZGND-4, from its singlet spin state, using the TB method. The rest of the information is same as that in Table III.

Peak	E (eV)	Transition Dipole (Å)		dominant contributing configurations
		$x-$pol	$y-$pol	
	0.00	1.5824	2.1315	$\|Z_1 \rightarrow Z_3\rangle$
	0.00	-3.2979	0.7503	$\|Z_1 \rightarrow Z_4\rangle$
	0.00	-0.9937	-0.1657	$\|Z_2 \rightarrow Z_3\rangle$
	0.00	-0.3700	2.3484	$\|Z_2 \rightarrow Z_4\rangle$
I	1.79	-0.2547	-1.4551	$\|(H-1)_1 \rightarrow Z_3\rangle$
		-0.1823	-0.3616	$\|(H-1)_1 \rightarrow Z_4\rangle$
		-1.1865	0.2021	$\|(H-1)_2 \rightarrow Z_3\rangle$
		-0.4777	0.6193	$\|(H-1)_2 \rightarrow Z_4\rangle$
		0.9430	-0.2459	$\|Z_1 \rightarrow (L+1)_1\rangle$
		0.4114	0.5568	$\|Z_1 \rightarrow (L+1)_2\rangle$
		0.3149	1.3125	$\|Z_2 \rightarrow (L+1)_1\rangle$
		-1.3873	0.2244	$\|Z_2 \rightarrow (L+1)_2\rangle$
II	2.12	-0.3320	-0.2405	$\|H-2 \rightarrow Z_3\rangle$
		-0.1172	0.6670	$\|H-2 \rightarrow Z_4\rangle$
		-0.6288	0.0236	$\|Z_1 \rightarrow L+2\rangle$
		-0.0862	-0.1531	$\|Z_2 \rightarrow L+2\rangle$
III	2.40	0.1200	-0.2433	$\|(H-3)_1 \rightarrow Z_3\rangle$
		-0.8825	-0.6075	$\|(H-3)_1 \rightarrow Z_4\rangle$
		-0.1155	0.5034	$\|(H-3)_2 \rightarrow Z_3\rangle$
		-0.3621	-0.1320	$\|(H-3)_2 \rightarrow Z_4\rangle$
		0.4915	-0.5042	$\|(H-3)_3 \rightarrow Z_3\rangle$
		-0.8388	0.3968	$\|(H-3)_3 \rightarrow Z_4\rangle$
		-0.3971	0.4226	$\|Z_1 \rightarrow (L+3)_1\rangle$
		-0.3574	-0.9561	$\|Z_1 \rightarrow (L+3)_2\rangle$
		-0.2314	0.6469	$\|Z_1 \rightarrow (L+3)_3\rangle$
		-0.4675	-0.3029	$\|Z_2 \rightarrow (L+3)_1\rangle$
		0.0759	-0.4049	$\|Z_2 \rightarrow (L+3)_2\rangle$
		0.6613	-0.0771	$\|Z_2 \rightarrow (L+3)_3\rangle$

Table XVII: Excitation energies as obtained in the linear optical absorption spectrum of TZGND-4, from its singlet spin state, using the TB method. The table contains the information corresponding to peaks IV and beyond, in continuation of the Table XVI. The rest of the information is same as that in Table III.

Peak	E (eV)	Transition Dipole (Å)		dominant contributing configurations
		$x-$pol	$y-$pol	
IV	3.18	-0.0265	0.1508	$\|H-5 \rightarrow Z_4\rangle$
		0.1421	-0.0053	$\|Z_1 \rightarrow L+5\rangle$
	3.21	-0.0664	-0.2795	$\|(H-6)_1 \rightarrow Z_3\rangle$
		0.2266	-0.0601	$\|(H-6)_2 \rightarrow Z_3\rangle$
		0.0901	-0.1254	$\|(H-6)_2 \rightarrow Z_4\rangle$
		-0.1701	0.0629	$\|Z_1 \rightarrow (L+6)_1\rangle$
		0.1056	0.1003	$\|Z_1 \rightarrow (L+6)_2\rangle$
		-0.0994	-0.2465	$\|Z_2 \rightarrow (L+6)_1\rangle$
		-0.2583	0.0799	$\|Z_2 \rightarrow (L+6)_2\rangle$
V	4.19	-0.1637	-0.0028	$\|(H-3)_1 \rightarrow (L+1)_1\rangle$
		-0.1729	-0.2782	$\|(H-3)_1 \rightarrow (L+1)_2\rangle$
		-0.0782	-0.1267	$\|(H-3)_2 \rightarrow (L+1)_1\rangle$
		-0.0954	0.1596	$\|(H-3)_2 \rightarrow (L+1)_2\rangle$
		-0.2765	0.1522	$\|(H-3)_3 \rightarrow (L+1)_1\rangle$
		-0.1814	-0.2847	$\|(H-1)_1 \rightarrow (L+3)_2\rangle$
		-0.1030	0.1432	$\|(H-1)_1 \rightarrow (L+3)_3\rangle$
		0.2615	-0.1623	$\|(H-1)_2 \rightarrow (L+3)_1\rangle$
		-0.1696	0.0289	$\|(H-1)_2 \rightarrow (L+3)_2\rangle$
		-0.0880	-0.1285	$\|(H-1)_2 \rightarrow (L+3)_3\rangle$
VII	4.52	-0.0791	-0.3710	$\|(H-3)_1 \rightarrow L+2\rangle$
		0.5457	-0.2203	$\|(H-3)_2 \rightarrow L+2\rangle$
		0.2222	0.4089	$\|(H-3)_3 \rightarrow L+2\rangle$
		-0.1997	-0.4447	$\|H-2 \rightarrow (L+3)_1\rangle$
		-0.0729	-0.3376	$\|H-2 \rightarrow (L+3)_2\rangle$
		0.5552	-0.2043	$\|H-2 \rightarrow (L+3)_3\rangle$

Table XVIII: Excitation energies as obtained in the linear optical absorption spectrum of TZGND-4, from its singlet spin state, using the TB method. The table contains the information corresponding to peaks VIII and beyond, in continuation of the Table XVII. The rest of the information is same as that in Table III.

Peak	E (eV)	Transition Dipole (Å)		dominant contributing configurations
		$x-$pol	$y-$pol	
VIII	4.72	-0.2022	-0.2505	$\|(H-4)_1 \rightarrow (L+1)_1\rangle$
		-0.2505	0.2022	$\|(H-4)_1 \rightarrow (L+1)_2\rangle$
		0.2505	-0.2022	$\|(H-4)_2 \rightarrow (L+1)_1\rangle$
		-0.2022	-0.2505	$\|(H-4)_2 \rightarrow (L+1)_2\rangle$
		0.1858	0.2629	$\|(H-1)_1 \rightarrow (L+4)_1\rangle$
		0.2629	-0.1858	$\|(H-1)_1 \rightarrow (L+4)_2\rangle$
		-0.2629	0.1858	$\|(H-1)_2 \rightarrow (L+4)_1\rangle$
		0.1858	0.2629	$\|(H-1)_2 \rightarrow (L+4)_2\rangle$
	4.80	0.2364	-0.2793	$\|(H-3)_1 \rightarrow (L+3)_1\rangle$
		0.4297	-0.2449	$\|(H-3)_1 \rightarrow (L+3)_2\rangle$
		-0.1927	0.1046	$\|(H-3)_1 \rightarrow (L+3)_3\rangle$
		-0.4001	-0.4715	$\|(H-3)_2 \rightarrow (L+3)_1\rangle$
		-0.1551	0.1245	$\|(H-3)_2 \rightarrow (L+3)_2\rangle$
		-0.3627	0.2814	$\|(H-3)_2 \rightarrow (L+3)_3\rangle$
		-0.2256	0.2576	$\|(H-3)_3 \rightarrow (L+3)_2\rangle$
		0.3624	0.4963	$\|(H-3)_3 \rightarrow (L+3)_3\rangle$
IX	5.61	0.1521	0.2216	$\|(H-6)_1 \rightarrow (L+3)_2\rangle$
		0.0859	-0.1049	$\|(H-6)_1 \rightarrow (L+3)_3\rangle$
		0.2060	-0.1307	$\|(H-6)_2 \rightarrow (L+3)_1\rangle$
		-0.1226	0.0392	$\|(H-6)_2 \rightarrow (L+3)_2\rangle$
		-0.0630	-0.1091	$\|(H-6)_2 \rightarrow (L+3)_3\rangle$
		-0.1079	0.0292	$\|(H-3)_1 \rightarrow (L+6)_1\rangle$
		0.1531	0.2169	$\|(H-3)_1 \rightarrow (L+6)_2\rangle$
		-0.0501	-0.1167	$\|(H-3)_2 \rightarrow (L+6)_1\rangle$
		0.0831	-0.1099	$\|(H-3)_2 \rightarrow (L+6)_2\rangle$
		-0.2169	0.1276	$\|(H-3)_3 \rightarrow (L+6)_1\rangle$
	5.84	0.0780	0.1347	$\|(H-4)_1 \rightarrow (L+4)_1\rangle$
		0.1347	-0.0780	$\|(H-4)_1 \rightarrow (L+4)_2\rangle$
		-0.1347	0.0780	$\|(H-4)_2 \rightarrow (L+4)_1\rangle$
		0.0780	0.1347	$\|(H-4)_2 \rightarrow (L+4)_2\rangle$

Table XIX: Excitation energies as obtained in the linear optical absorption spectrum of TZGND-4, from its singlet spin state, using the TB method. The table contains the information corresponding to peaks X and beyond, in continuation of the Table XVIII. The rest of the information is same as that in Table III.

Peak	E (eV)	Transition Dipole (Å)		dominant contributing configurations
		$x-$pol	$y-$pol	
X	6.10	-0.1239	0.2154	$\|H-5 \rightarrow (L+4)_1\rangle$
		0.2154	-0.1239	$\|H-5 \rightarrow (L+4)_2\rangle$
		0.2152	-0.1244	$\|(H-4)_1 \rightarrow L+5\rangle$
		-0.1244	-0.2152	$\|(H-4)_2 \rightarrow L+5\rangle$
	6.13	-0.1073	-0.1784	$\|(H-6)_1 \rightarrow (L+4)_1\rangle$
		-0.1784	0.1073	$\|(H-6)_1 \rightarrow (L+4)_2\rangle$
		-0.1784	0.1073	$\|(H-6)_2 \rightarrow (L+4)_1\rangle$
		0.1073	0.1784	$\|(H-6)_2 \rightarrow (L+4)_2\rangle$
		-0.1062	-0.1791	$\|(H-4)_1 \rightarrow (L+6)_1\rangle$
		0.1791	-0.1062	$\|(H-4)_1 \rightarrow (L+6)_2\rangle$
		0.1791	-0.1062	$\|(H-4)_2 \rightarrow (L+6)_1\rangle$
		0.1062	0.1791	$\|(H-4)_2 \rightarrow (L+6)_2\rangle$
XI	6.40	-0.3266	0.1815	$\|(H-6)_1 \rightarrow L+5\rangle$
		-0.1815	-0.3266	$\|(H-6)_2 \rightarrow L+5\rangle$
		0.1829	0.3258	$\|H-5 \rightarrow (L+6)_1\rangle$
		0.3258	-0.1829	$\|H-5 \rightarrow (L+6)_2\rangle$

Table XX: Excitation energies as obtained in the linear optical absorption spectrum of TZGND-4, from its triplet spin state, using the TB method. The rest of the information is same as that in Table III.

Peak	E (eV)	Transition Dipole (Å)		dominant contributing configurations
		$x-$pol	$y-$pol	
	0.00	-0.9052	0.5005	$\|Z_1 \rightarrow Z_2\rangle$
	0.00	1.5824	2.1315	$\|Z_1 \rightarrow Z_3\rangle$
	0.00	-3.2979	0.7503	$\|Z_1 \rightarrow Z_4\rangle$
	0.00	-0.3700	2.3484	$\|Z_2 \rightarrow Z_4\rangle$
	0.00	0.5736	1.0995	$\|Z_3 \rightarrow Z_4\rangle$
I	1.79	-1.3635	0.3106	$\|(H-1)_1 \rightarrow Z_2\rangle$
		-0.2547	-1.4551	$\|(H-1)_1 \rightarrow Z_3\rangle$
		-0.1823	-0.3616	$\|(H-1)_1 \rightarrow Z_4\rangle$
		0.4058	1.2949	$\|(H-1)_2 \rightarrow Z_2\rangle$
		-1.1865	0.2021	$\|(H-1)_2 \rightarrow Z_3\rangle$
		-0.4777	0.6193	$\|(H-1)_2 \rightarrow Z_4\rangle$
		0.9430	-0.2459	$\|Z_1 \rightarrow (L+1)_1\rangle$
		0.4114	0.5568	$\|Z_1 \rightarrow (L+1)_2\rangle$
		0.3149	1.3125	$\|Z_2 \rightarrow (L+1)_1\rangle$
		-1.3873	0.2244	$\|Z_2 \rightarrow (L+1)_2\rangle$
		-1.2007	0.1056	$\|Z_3 \rightarrow (L+1)_1\rangle$
		-0.1758	-1.4653	$\|Z_3 \rightarrow (L+1)_2\rangle$
II	2.12	-0.0862	-0.1531	$\|H-2 \rightarrow Z_2\rangle$
		-0.3320	-0.2405	$\|H-2 \rightarrow Z_3\rangle$
		-0.1172	0.6670	$\|H-2 \rightarrow Z_4\rangle$
		-0.6288	0.0236	$\|Z_1 \rightarrow L+2\rangle$
		-0.0862	-0.1531	$\|Z_2 \rightarrow L+2\rangle$
		-0.3320	-0.2405	$\|Z_3 \rightarrow L+2\rangle$

Table XXI: Excitation energies as obtained in the linear optical absorption spectrum of TZGND-4, from its triplet spin state, using the TB method. The table contains the information corresponding to peaks III and beyond, in continuation of the Table XX. The rest of the information is same as that in Table III.

Peak	E (eV)	Transition Dipole (Å)		dominant contributing configurations
		$x-$pol	$y-$pol	
III	2.4	0.0519	-0.4264	$\|(H-3)_1 \rightarrow Z_2\rangle$
		0.1200	-0.2433	$\|(H-3)_1 \rightarrow Z_3\rangle$
		-0.8825	-0.6075	$\|(H-3)_1 \rightarrow Z_4\rangle$
		0.6356	-0.0851	$\|(H-3)_2 \rightarrow Z_2\rangle$
		-0.1155	0.5034	$\|(H-3)_2 \rightarrow Z_3\rangle$
		-0.3621	-0.1320	$\|(H-3)_2 \rightarrow Z_4\rangle$
		0.5050	0.2695	$\|(H-3)_3 \rightarrow Z_2\rangle$
		0.4915	-0.5042	$\|(H-3)_3 \rightarrow Z_3\rangle$
		-0.8388	0.3968	$\|(H-3)_3 \rightarrow Z_4\rangle$
		-0.3971	0.4226	$\|Z_1 \rightarrow (L+3)_1\rangle$
		-0.3574	-0.9561	$\|Z_1 \rightarrow (L+3)_2\rangle$
		-0.2314	0.6469	$\|Z_1 \rightarrow (L+3)_3\rangle$
		-0.4675	-0.3029	$\|Z_2 \rightarrow (L+3)_1\rangle$
		0.0759	-0.4049	$\|Z_2 \rightarrow (L+3)_2\rangle$
		0.6613	-0.0771	$\|Z_2 \rightarrow (L+3)_3\rangle$
		-0.4869	0.5103	$\|Z_3 \rightarrow (L+3)_1\rangle$
		0.1561	-0.2868	$\|Z_3 \rightarrow (L+3)_2\rangle$
		-0.0885	0.4735	$\|Z_3 \rightarrow (L+3)_3\rangle$

Table XXII: Excitation energies as obtained in the linear optical absorption spectrum of TZGND-4, from its triplet spin state, using the TB method. The table contains the information corresponding to peaks IV and beyond, in continuation of the Table XXI. The rest of the information is same as that in Table III.

Peak	E (eV)	Transition Dipole (Å)		dominant contributing configurations
		$x-$pol	$y-$pol	
IV	3.18	-0.0265	0.1508	$\|H-5 \rightarrow Z_4\rangle$
		0.1421	-0.0053	$\|Z_1 \rightarrow L+5\rangle$
	3.21	-0.2588	0.0788	$\|(H-6)_1 \rightarrow Z_2\rangle$
		-0.0664	-0.2795	$\|(H-6)_1 \rightarrow Z_3\rangle$
		-0.0983	-0.2468	$\|(H-6)_2 \rightarrow Z_2\rangle$
		0.2266	-0.0601	$\|(H-6)_2 \rightarrow Z_3\rangle$
		0.0901	-0.1254	$\|(H-6)_2 \rightarrow Z_4\rangle$
		-0.1701	0.0629	$\|Z_1 \rightarrow (L+6)_1\rangle$
		0.1056	0.1003	$\|Z_1 \rightarrow (L+6)_2\rangle$
		-0.0994	-0.2465	$\|Z_2 \rightarrow (L+6)_1\rangle$
		-0.2583	0.0799	$\|Z_2 \rightarrow (L+6)_2\rangle$
		0.2263	-0.0613	$\|Z_3 \rightarrow (L+6)_1\rangle$
		-0.0674	-0.2792	$\|Z_3 \rightarrow (L+6)_2\rangle$

Table XXIII: Excitation energies as obtained in the linear optical absorption spectrum of TZGND-4, from its triplet spin state, using the TB method. The table contains the information corresponding to peaks V and beyond, in continuation of the Table XXII. The rest of the information is same as that in Table III.

Peak	E (eV)	Transition Dipole (Å)		dominant contributing configurations
		$x-$pol	$y-$pol	
V	4.19	-0.1637	-0.0028	$\|(H-3)_1 \rightarrow (L+1)_1\rangle$
		-0.1729	-0.2782	$\|(H-3)_1 \rightarrow (L+1)_2\rangle$
		-0.0782	-0.1267	$\|(H-3)_2 \rightarrow (L+1)_1\rangle$
		-0.0954	0.1596	$\|(H-3)_2 \rightarrow (L+1)_2\rangle$
		-0.2765	0.1522	$\|(H-3)_3 \rightarrow (L+1)_1\rangle$
		-0.1814	-0.2847	$\|(H-1)_1 \rightarrow (L+3)_2\rangle$
		-0.1030	0.1432	$\|(H-1)_1 \rightarrow (L+3)_3\rangle$
		0.2615	-0.1623	$\|(H-1)_2 \rightarrow (L+3)_1\rangle$
		-0.1696	0.0289	$\|(H-1)_2 \rightarrow (L+3)_2\rangle$
		-0.0880	-0.1285	$\|(H-1)_2 \rightarrow (L+3)_3\rangle$
VII	4.52	-0.0791	-0.3710	$\|(H-3)_1 \rightarrow L+2\rangle$
		0.5457	-0.2203	$\|(H-3)_2 \rightarrow L+2\rangle$
		0.2222	0.4089	$\|(H-3)_3 \rightarrow L+2\rangle$
		-0.1997	-0.4447	$\|H-2 \rightarrow (L+3)_1\rangle$
		-0.0729	-0.3376	$\|H-2 \rightarrow (L+3)_2\rangle$
		0.5552	-0.2043	$\|H-2 \rightarrow (L+3)_3\rangle$
VIII	4.72	-0.2022	-0.2505	$\|(H-4)_1 \rightarrow (L+1)_1\rangle$
		-0.2505	0.2022	$\|(H-4)_1 \rightarrow (L+1)_2\rangle$
		0.2505	-0.2022	$\|(H-4)_2 \rightarrow (L+1)_1\rangle$
		-0.2022	-0.2505	$\|(H-4)_2 \rightarrow (L+1)_2\rangle$
		0.1858	0.2629	$\|(H-1)_1 \rightarrow (L+4)_1\rangle$
		0.2629	-0.1858	$\|(H-1)_1 \rightarrow (L+4)_2\rangle$
		-0.2629	0.1858	$\|(H-1)_2 \rightarrow (L+4)_1\rangle$
		0.1858	0.2629	$\|(H-1)_2 \rightarrow (L+4)_2\rangle$

Table XXIV: Excitation energies as obtained in the linear optical absorption spectrum of TZGND-4, from its triplet spin state, using the TB method. The table contains the information corresponding to peaks VIII and beyond, in continuation of the Table XXIII. The rest of the information is same as that in Table III.

Peak	E (eV)	Transition Dipole (Å)		dominant contributing configurations
		$x-$pol	$y-$pol	
VIII	4.80	0.2364	-0.2793	$\|(H-3)_1 \rightarrow (L+3)_1\rangle$
		0.4297	-0.2449	$\|(H-3)_1 \rightarrow (L+3)_2\rangle$
		-0.1927	0.1046	$\|(H-3)_1 \rightarrow (L+3)_3\rangle$
		-0.4001	-0.4715	$\|(H-3)_2 \rightarrow (L+3)_1\rangle$
		-0.1551	0.1245	$\|(H-3)_2 \rightarrow (L+3)_2\rangle$
		-0.3627	0.2814	$\|(H-3)_2 \rightarrow (L+3)_3\rangle$
		-0.2256	0.2576	$\|(H-3)_3 \rightarrow (L+3)_2\rangle$
		0.3624	0.4963	$\|(H-3)_3 \rightarrow (L+3)_3\rangle$
IX	5.61	0.1521	0.2216	$\|(H-6)_1 \rightarrow (L+3)_2\rangle$
		0.0859	-0.1049	$\|(H-6)_1 \rightarrow (L+3)_3\rangle$
		0.2060	-0.1307	$\|(H-6)_2 \rightarrow (L+3)_1\rangle$
		-0.1226	0.0392	$\|(H-6)_2 \rightarrow (L+3)_2\rangle$
		-0.0630	-0.1091	$\|(H-6)_2 \rightarrow (L+3)_3\rangle$
		-0.1079	0.0292	$\|(H-3)_1 \rightarrow (L+6)_1\rangle$
		0.1531	0.2169	$\|(H-3)_1 \rightarrow (L+6)_2\rangle$
		-0.0501	-0.1167	$\|(H-3)_2 \rightarrow (L+6)_1\rangle$
		0.0831	-0.1099	$\|(H-3)_2 \rightarrow (L+6)_2\rangle$
		-0.2169	0.1276	$\|(H-3)_3 \rightarrow (L+6)_1\rangle$
	5.84	0.0780	0.1347	$\|(H-4)_1 \rightarrow (L+4)_1\rangle$
		0.1347	-0.0780	$\|(H-4)_1 \rightarrow (L+4)_2\rangle$
		-0.1347	0.0780	$\|(H-4)_2 \rightarrow (L+4)_1\rangle$
		0.0780	0.1347	$\|(H-4)_2 \rightarrow (L+4)_2\rangle$
X	6.10	-0.1239	0.2154	$\|H-5 \rightarrow (L+4)_1\rangle$
		0.2154	-0.1239	$\|H-5 \rightarrow (L+4)_2\rangle$
		0.2152	-0.1244	$\|(H-4)_1 \rightarrow L+5\rangle$
		-0.1244	-0.2152	$\|(H-4)_2 \rightarrow L+5\rangle$

Table XXV: Excitation energies as obtained in the linear optical absorption spectrum of TZGND-4, from its triplet spin state, using the TB method. The table contains the information corresponding to peaks X and beyond, in continuation of the Table XXIV. The rest of the information is same as that in Table III.

Peak	E (eV)	Transition Dipole (Å)		dominant contributing configurations
		$x-$pol	$y-$pol	
X	6.13	-0.1073	-0.1784	$\|(H-6)_1 \rightarrow (L+4)_1\rangle$
		-0.1784	0.1073	$\|(H-6)_1 \rightarrow (L+4)_2\rangle$
		-0.1784	0.1073	$\|(H-6)_2 \rightarrow (L+4)_1\rangle$
		0.1073	0.1784	$\|(H-6)_2 \rightarrow (L+4)_2\rangle$
		-0.1062	-0.1791	$\|(H-4)_1 \rightarrow (L+6)_1\rangle$
		0.1791	-0.1062	$\|(H-4)_1 \rightarrow (L+6)_2\rangle$
		0.1791	-0.1062	$\|(H-4)_2 \rightarrow (L+6)_1\rangle$
		0.1062	0.1791	$\|(H-4)_2 \rightarrow (L+6)_2\rangle$
XI	6.40	-0.3266	0.1815	$\|(H-6)_1 \rightarrow L+5\rangle$
		-0.1815	-0.3266	$\|(H-6)_2 \rightarrow L+5\rangle$
		0.1829	0.3258	$\|H-5 \rightarrow (L+6)_1\rangle$
		0.3258	-0.1829	$\|H-5 \rightarrow (L+6)_2\rangle$

Table XXVI: Excitation energies as obtained in the linear optical absorption spectrum of TZGND-4, from its quintet spin state, using the TB method. The rest of the information is same as that in Table III.

Peak	E (eV)	Transition Dipole (Å)		dominant contributing configurations
		$x-$pol	$y-$pol	
I	1.79	0.4728	0.5394	$\|(H-1)_1 \rightarrow Z_1\rangle$
		-1.3635	0.3106	$\|(H-1)_1 \rightarrow Z_2\rangle$
		-0.2547	-1.4551	$\|(H-1)_1 \rightarrow Z_3\rangle$
		-0.1823	-0.3616	$\|(H-1)_1 \rightarrow Z_4\rangle$
		0.9138	-0.2821	$\|(H-1)_2 \rightarrow Z_1\rangle$
		0.4058	1.2949	$\|(H-1)_2 \rightarrow Z_2\rangle$
		-1.1865	0.2021	$\|(H-1)_2 \rightarrow Z_3\rangle$
		-0.4777	0.6193	$\|(H-1)_2 \rightarrow Z_4\rangle$
		0.9430	-0.2459	$\|Z_1 \rightarrow (L+1)_1\rangle$
		0.4114	0.5568	$\|Z_1 \rightarrow (L+1)_2\rangle$
		0.3149	1.3125	$\|Z_2 \rightarrow (L+1)_1\rangle$
		-1.3873	0.2244	$\|Z_2 \rightarrow (L+1)_2\rangle$
		-1.2007	0.1056	$\|Z_3 \rightarrow (L+1)_1\rangle$
		-0.1758	-1.4653	$\|Z_3 \rightarrow (L+1)_2\rangle$
		-0.4887	0.5941	$\|Z_4 \rightarrow (L+1)_1\rangle$
		-0.1503	-0.4017	$\|Z_4 \rightarrow (L+1)_2\rangle$
II	2.12	-0.6288	0.0236	$\|H-2 \rightarrow Z_1\rangle$
		-0.0862	-0.1531	$\|H-2 \rightarrow Z_2\rangle$
		-0.3320	-0.2405	$\|H-2 \rightarrow Z_3\rangle$
		-0.1172	0.6670	$\|H-2 \rightarrow Z_4\rangle$
		-0.6288	0.0236	$\|Z_1 \rightarrow L+2\rangle$
		-0.0862	-0.1531	$\|Z_2 \rightarrow L+2\rangle$
		-0.3320	-0.2405	$\|Z_3 \rightarrow L+2\rangle$
		-0.1172	0.6670	$\|Z_4 \rightarrow L+2\rangle$

Table XXVII: Excitation energies as obtained in the linear optical absorption spectrum of TZGND-4, from its quintet spin state, using the TB method. The table contains the information corresponding to peaks III and beyond, in continuation of the Table XXVI. The rest of the information is same as that in Table III.

Peak	E (eV)	Transition Dipole (Å)		dominant contributing configurations
		$x-$pol	$y-$pol	
III	2.4	-0.3878	-0.9146	$\|(H-3)_1 \rightarrow Z_1\rangle$
		0.0519	-0.4264	$\|(H-3)_1 \rightarrow Z_2\rangle$
		0.1200	-0.2433	$\|(H-3)_1 \rightarrow Z_3\rangle$
		-0.8825	-0.6075	$\|(H-3)_1 \rightarrow Z_4\rangle$
		-0.2447	0.6839	$\|(H-3)_2 \rightarrow Z_1\rangle$
		0.6356	-0.0851	$\|(H-3)_2 \rightarrow Z_2\rangle$
		-0.1155	0.5034	$\|(H-3)_2 \rightarrow Z_3\rangle$
		-0.3621	-0.1320	$\|(H-3)_2 \rightarrow Z_4\rangle$
		0.3587	-0.4548	$\|(H-3)_3 \rightarrow Z_1\rangle$
		0.5050	0.2695	$\|(H-3)_3 \rightarrow Z_2\rangle$
		0.4915	-0.5042	$\|(H-3)_3 \rightarrow Z_3\rangle$
		-0.8388	0.3968	$\|(H-3)_3 \rightarrow Z_4\rangle$
		-0.3971	0.4226	$\|Z_1 \rightarrow (L+3)_1\rangle$
		-0.3574	-0.9561	$\|Z_1 \rightarrow (L+3)_2\rangle$
		-0.2314	0.6469	$\|Z_1 \rightarrow (L+3)_3\rangle$
		-0.4675	-0.3029	$\|Z_2 \rightarrow (L+3)_1\rangle$
		0.0759	-0.4049	$\|Z_2 \rightarrow (L+3)_2\rangle$
		0.6613	-0.0771	$\|Z_2 \rightarrow (L+3)_3\rangle$
		-0.4869	0.5103	$\|Z_3 \rightarrow (L+3)_1\rangle$
		0.1561	-0.2868	$\|Z_3 \rightarrow (L+3)_2\rangle$
		-0.0885	0.4735	$\|Z_3 \rightarrow (L+3)_3\rangle$
		0.7550	-0.4449	$\|Z_4 \rightarrow (L+3)_1\rangle$
		-0.9326	-0.5758	$\|Z_4 \rightarrow (L+3)_2\rangle$
		-0.4169	-0.1200	$\|Z_4 \rightarrow (L+3)_3\rangle$

Table XXVIII: Excitation energies as obtained in the linear optical absorption spectrum of TZGND-4, from its quintet spin state, using the TB method. The table contains the information corresponding to peaks IV and beyond, in continuation of the Table XXVII. The rest of the information is same as that in Table III.

Peak	E (eV)	Transition Dipole (Å)		dominant contributing configurations
		$x-$pol	$y-$pol	
IV	3.21	0.1048	0.1006	$\|(H-6)_1 \rightarrow Z_1\rangle$
		-0.2588	0.0788	$\|(H-6)_1 \rightarrow Z_2\rangle$
		-0.0664	-0.2795	$\|(H-6)_1 \rightarrow Z_3\rangle$
		-0.1705	0.0625	$\|(H-6)_2 \rightarrow Z_1\rangle$
		-0.0983	-0.2468	$\|(H-6)_2 \rightarrow Z_2\rangle$
		0.2266	-0.0601	$\|(H-6)_2 \rightarrow Z_3\rangle$
		0.0901	-0.1254	$\|(H-6)_2 \rightarrow Z_4\rangle$
		-0.1701	0.0629	$\|Z_1 \rightarrow (L+6)_1\rangle$
		0.1056	0.1003	$\|Z_1 \rightarrow (L+6)_2\rangle$
		-0.0994	-0.2465	$\|Z_2 \rightarrow (L+6)_1\rangle$
		-0.2583	0.0799	$\|Z_2 \rightarrow (L+6)_2\rangle$
		0.2263	-0.0613	$\|Z_3 \rightarrow (L+6)_1\rangle$
		-0.0674	-0.2792	$\|Z_3 \rightarrow (L+6)_2\rangle$
		0.0899	-0.1256	$\|Z_4 \rightarrow (L+6)_1\rangle$
V	3.91	-0.2197	-0.5707	$\|H-2 \rightarrow (L+1)_1\rangle$
		0.5707	-0.2197	$\|H-2 \rightarrow (L+1)_2\rangle$
		0.5549	-0.2569	$\|(H-1)_1 \rightarrow L+2\rangle$
		-0.2569	-0.5549	$\|(H-1)_2 \rightarrow L+2\rangle$
VI	4.19	-0.1637	-0.0028	$\|(H-3)_1 \rightarrow (L+1)_1\rangle$
		-0.1729	-0.2782	$\|(H-3)_1 \rightarrow (L+1)_2\rangle$
		-0.0782	-0.1267	$\|(H-3)_2 \rightarrow (L+1)_1\rangle$
		-0.0954	0.1596	$\|(H-3)_2 \rightarrow (L+1)_2\rangle$
		-0.2765	0.1522	$\|(H-3)_3 \rightarrow (L+1)_1\rangle$
		-0.1814	-0.2847	$\|(H-1)_1 \rightarrow (L+3)_2\rangle$
		-0.1030	0.1432	$\|(H-1)_1 \rightarrow (L+3)_3\rangle$
		0.2615	-0.1623	$\|(H-1)_2 \rightarrow (L+3)_1\rangle$
		-0.1696	0.0289	$\|(H-1)_2 \rightarrow (L+3)_2\rangle$
		-0.0880	-0.1285	$\|(H-1)_2 \rightarrow (L+3)_3\rangle$

Table XXIX: Excitation energies as obtained in the linear optical absorption spectrum of TZGND-4, from its quintet spin state, using the TB method. The table contains the information corresponding to peaks VII and beyond, in continuation of the Table XXVIII. The rest of the information is same as that in Table III.

Peak	E (eV)	Transition Dipole (Å)		dominant contributing configurations
		$x-$pol	$y-$pol	
VII	4.52	-0.0791	-0.3710	$\|(H-3)_1 \rightarrow L+2\rangle$
		0.5457	-0.2203	$\|(H-3)_2 \rightarrow L+2\rangle$
		0.2222	0.4089	$\|(H-3)_3 \rightarrow L+2\rangle$
		-0.1997	-0.4447	$\|H-2 \rightarrow (L+3)_1\rangle$
		-0.0729	-0.3376	$\|H-2 \rightarrow (L+3)_2\rangle$
		0.5552	-0.2043	$\|H-2 \rightarrow (L+3)_3\rangle$
VIII	4.72	-0.2022	-0.2505	$\|(H-4)_1 \rightarrow (L+1)_1\rangle$
		-0.2505	0.2022	$\|(H-4)_1 \rightarrow (L+1)_2\rangle$
		0.2505	-0.2022	$\|(H-4)_2 \rightarrow (L+1)_1\rangle$
		-0.2022	-0.2505	$\|(H-4)_2 \rightarrow (L+1)_2\rangle$
		0.1858	0.2629	$\|(H-1)_1 \rightarrow (L+4)_1\rangle$
		0.2629	-0.1858	$\|(H-1)_1 \rightarrow (L+4)_2\rangle$
		-0.2629	0.1858	$\|(H-1)_2 \rightarrow (L+4)_1\rangle$
		0.1858	0.2629	$\|(H-1)_2 \rightarrow (L+4)_2\rangle$
	4.80	0.2364	-0.2793	$\|(H-3)_1 \rightarrow (L+3)_1\rangle$
		0.4297	-0.2449	$\|(H-3)_1 \rightarrow (L+3)_2\rangle$
		-0.1927	0.1046	$\|(H-3)_1 \rightarrow (L+3)_3\rangle$
		-0.4001	-0.4715	$\|(H-3)_2 \rightarrow (L+3)_1\rangle$
		-0.1551	0.1245	$\|(H-3)_2 \rightarrow (L+3)_2\rangle$
		-0.3627	0.2814	$\|(H-3)_2 \rightarrow (L+3)_3\rangle$
		-0.2256	0.2576	$\|(H-3)_3 \rightarrow (L+3)_2\rangle$
		0.3624	0.4963	$\|(H-3)_3 \rightarrow (L+3)_3\rangle$

Table XXX: Excitation energies as obtained in the linear optical absorption spectrum of TZGND-4, from its quintet spin state, using the TB method. The table contains the information corresponding to peaks IX and beyond, in continuation of the Table XXIX. The rest of the information is same as that in Table III.

Peak	E (eV)	Transition Dipole (Å)		dominant contributing configurations
		$x-$pol	$y-$pol	
IX	5.61	0.1521	0.2216	$\|(H-6)_1 \rightarrow (L+3)_2\rangle$
		0.0859	-0.1049	$\|(H-6)_1 \rightarrow (L+3)_3\rangle$
		0.2060	-0.1307	$\|(H-6)_2 \rightarrow (L+3)_1\rangle$
		-0.1226	0.0392	$\|(H-6)_2 \rightarrow (L+3)_2\rangle$
		-0.0630	-0.1091	$\|(H-6)_2 \rightarrow (L+3)_3\rangle$
		-0.1079	0.0292	$\|(H-3)_1 \rightarrow (L+6)_1\rangle$
		0.1531	0.2169	$\|(H-3)_1 \rightarrow (L+6)_2\rangle$
		-0.0501	-0.1167	$\|(H-3)_2 \rightarrow (L+6)_1\rangle$
		0.0831	-0.1099	$\|(H-3)_2 \rightarrow (L+6)_2\rangle$
		-0.2169	0.1276	$\|(H-3)_3 \rightarrow (L+6)_1\rangle$
	5.84	0.0780	0.1347	$\|(H-4)_1 \rightarrow (L+4)_1\rangle$
		0.1347	-0.0780	$\|(H-4)_1 \rightarrow (L+4)_2\rangle$
		-0.1347	0.0780	$\|(H-4)_2 \rightarrow (L+4)_1\rangle$
		0.0780	0.1347	$\|(H-4)_2 \rightarrow (L+4)_2\rangle$

Table XXXI: Excitation energies as obtained in the linear optical absorption spectrum of TZGND-4, from its quintet spin state, using the TB method. The table contains the information corresponding to peaks X and beyond, in continuation of the Table XXX. The rest of the information is same as that in Table III.

Peak	E (eV)	Transition Dipole (Å)		dominant contributing configurations
		$x-$pol	$y-$pol	
X	6.10	-0.1239	0.2154	$\|H-5 \rightarrow (L+4)_1\rangle$
		0.2154	-0.1239	$\|H-5 \rightarrow (L+4)_2\rangle$
		0.2152	-0.1244	$\|(H-4)_1 \rightarrow L+5\rangle$
		-0.1244	-0.2152	$\|(H-4)_2 \rightarrow L+5\rangle$
	6.13	-0.1073	-0.1784	$\|(H-6)_1 \rightarrow (L+4)_1\rangle$
		-0.1784	0.1073	$\|(H-6)_1 \rightarrow (L+4)_2\rangle$
		-0.1784	0.1073	$\|(H-6)_2 \rightarrow (L+4)_1\rangle$
		0.1073	0.1784	$\|(H-6)_2 \rightarrow (L+4)_2\rangle$
		-0.1062	-0.1791	$\|(H-4)_1 \rightarrow (L+6)_1\rangle$
		0.1791	-0.1062	$\|(H-4)_1 \rightarrow (L+6)_2\rangle$
		0.1791	-0.1062	$\|(H-4)_2 \rightarrow (L+6)_1\rangle$
		0.1062	0.1791	$\|(H-4)_2 \rightarrow (L+6)_2\rangle$
XI	6.40	-0.3266	0.1815	$\|(H-6)_1 \rightarrow L+5\rangle$
		-0.1815	-0.3266	$\|(H-6)_2 \rightarrow L+5\rangle$
		0.1829	0.3258	$\|H-5 \rightarrow (L+6)_1\rangle$
		0.3258	-0.1829	$\|H-5 \rightarrow (L+6)_2\rangle$

WAVE FUNCTION ANALYSIS - CORRELATED CALCULATIONS

The following tables (XXXII–XLIX) contain the detailed information about the configurations contributing to the peaks in the absorption spectra of TZGNDs at CI level (*cf.* Figure 5).

Table XXXII: Excitation energies as obtained in the linear optical absorption spectrum of TZGND-1, from its doublet spin state, using the MRSDCI method coupled with the standard parameters in the PPP model Hamiltonian. The table contains dominant contributing configurations, excitation energies, transition dipole moments, of the different excited states corresponding to the various peaks of the spectrum, with respect to the reference state (RS). RS corresponds to an open shell configuration, denoted by singly occupied state/states (Z's), where the closed shell contribution to the RS has not been not shown. DF represents the dipole forbidden state.

Peak	State	E (eV)	Transition Dipole (Å)	dominant contributing configurations
RS	1^2B_2			$\|Z\rangle$ (0.8531)
DF	1^2A_1	2.21	-	$\|Z \rightarrow (L+1)_1\rangle$ (-0.5976)
				$\|(H-2)_1 \rightarrow Z\rangle$ (0.5822)
DF	2^2B_2	2.21	-	$\|Z \rightarrow (L+1)_2\rangle$ (-0.5976)
				$\|(H-2)_2 \rightarrow Z\rangle$ (0.5822)
I	5^2A_1	4.00	0.847	$\|(H-2)_1 \rightarrow Z\rangle$ (0.6095)
				$\|Z \rightarrow (L+1)_1\rangle$ (0.5675)
I	4^2B_2	4.00	0.848	$\|(H-2)_2 \rightarrow Z\rangle$ (-0.6095)
				$\|Z \rightarrow (L+1)_2\rangle$ (-0.5675)
II	10^2A_1	5.83	0.218	$\|(H-3)_1 \rightarrow Z\rangle$ (-0.5217)
				$\|Z \rightarrow (L+3)_1\rangle$ (-0.5017)
II	10^2B_2	5.83	0.218	$\|(H-3)_2 \rightarrow Z\rangle$ (-0.5218)
				$\|Z \rightarrow (L+3)_2\rangle$ (0.5013)
III	12^2A_1	6.24	0.938	$\|(H-2)_2 \rightarrow L+2\rangle$ (0.4937)
				$\|H-1 \rightarrow (L+1)_2\rangle$ (0.4743)
III	12^2B_2	6.24	0.941	$\|(H-2)_1 \rightarrow L+2\rangle$ (0.4941)
				$\|H-1 \rightarrow (L+1)_1\rangle$ (0.4750)
IV	15^2A_1	6.47	0.548	$\|(H-2)_2 \rightarrow (L+1)_1\rangle$ (0.5656)
				$\|(H-2)_1 \rightarrow (L+1)_2\rangle$ (0.5651)
IV	16^2B_2	6.47	0.541	$\|(H-2)_1 \rightarrow (L+1)_1\rangle$ (0.5723)
				$\|(H-2)_2 \rightarrow (L+1)_2\rangle$ (0.5564)
V	18^2A_1	6.73	0.970	$\|H-1 \rightarrow (L+1)_2\rangle$ (0.5239)
				$\|(H-2)_2 \rightarrow L+1\rangle$ (0.5136)
V	18^2B_2	6.73	0.971	$\|H-1 \rightarrow (L+1)_1\rangle$ (0.5239)
				$\|(H-2)_1 \rightarrow L+2\rangle$ (0.5139)

Table XXXIII: Excitation energies as obtained in the linear optical absorption spectrum of TZGND-1, from its doublet spin state, using the MRSDCI method coupled with the standard parameters in the PPP model Hamiltonian. The table contains the information corresponding to peaks VI and beyond, in continuation to the Table. XXXII. The rest of the information is same as that in Table XXXII.

Peak	State	E (eV)	Transition Dipole (Å)	dominant contributing configurations
VI	25^2A_1	7.52	0.327	$\|(H-3)_2 \rightarrow (L+1)_1\rangle$ (0.2869)
				$\|(H-3)_1 \rightarrow (L+1)_2\rangle$ (0.2857)
VI	24^2B_2	7.52	0.327	$\|(H-3)_2 \rightarrow (L+1)_2\rangle$ (0.2875)
				$\|(H-3)_1 \rightarrow (L+1)_1\rangle$ (0.2867)
VII	28^2A_1	7.74	0.207	$\|(H-3)_2 \rightarrow L+2\rangle$ (0.3159)
				$\|H-1 \rightarrow (L+3)_2\rangle$ (0.3128)
VII	28^2B_2	7.74	0.212	$\|(H-3)_1 \rightarrow L+2\rangle$ (0.3142)
				$\|H-1 \rightarrow (L+3)_1\rangle$ (0.3131)
VIII	37^2A_1	8.18	0.227	$\|Z \rightarrow L+2;\ H-1 \rightarrow (L+1)_1\rangle$ (0.3411)
				$\|(H-2)_1 \rightarrow Z;\ H-1 \rightarrow L+2\rangle$ (0.3281)
VIII	35^2B_2	8.18	0.216	$\|H-1 \rightarrow L+2;\ Z \rightarrow (L+1)_2\rangle$ (0.3250)
				$\|H-1 \rightarrow L+2;\ (H-2)_2 \rightarrow Z\rangle$ (0.3113)

Table XXXIV: Excitation energies as obtained in the linear optical absorption spectrum of TZGND-1, from its doublet spin state, using the MRSDCI method coupled with the screened parameters in the PPP model Hamiltonian. The rest of the information is same as that in Table XXXII.

Peak	State	E (eV)	Transition Dipole (Å)	dominant contributing configurations
RS	1^2B_2			$\|Z\rangle$ (0.7459)
DF	1^2A_1	1.98	-	$\|Z \rightarrow (L+1)_1\rangle$ (0.5474)
				$\|(H-2)_1 \rightarrow Z\rangle$ (0.4922)
DF	2^2B_2	1.98	-	$\|Z \rightarrow (L+1)_2\rangle$ (−0.5475)
				$\|(H-2)_2 \rightarrow Z\rangle$ (0.4921)
I	5^2A_1	3.86	1.059	$\|Z \rightarrow (L+1)_1\rangle$ (−0.5556)
				$\|(H-2)_1 \rightarrow Z\rangle$ (0.5447)
I	4^2B_2	3.86	1.059	$\|Z \rightarrow (L+1)_2\rangle$ (−0.5552)
				$\|(H-2)_2 \rightarrow Z\rangle$ (−0.5449)
II	11^2A_1	5.44	0.341	$\|Z \rightarrow (L+3)_1\rangle$ (0.4735)
				$\|(H-3)_1 \rightarrow Z\rangle$ (−0.4595)
II	10^2B_2	5.44	0.346	$\|Z \rightarrow (L+3)_2\rangle$ (0.4741)
				$\|(H-3)_2 \rightarrow Z\rangle$ (0.4598)
III	12^2A_1	5.73	1.008	$\|(H-2)_2 \rightarrow L+2\rangle$ (0.4776)
				$\|H-1 \rightarrow (L+1)_2\rangle$ (0.4634)
III	12^2B_2	5.73	1.002	$\|(H-2)_1 \rightarrow L+2\rangle$ (0.4804)
				$\|H-1 \rightarrow (L+1)_1\rangle$ (0.4630)
IV	16^2A_1	6.09	0.398	$\|(H-2)_2 \rightarrow (L+1)_1\rangle$ (0.4294)
				$\|(H-2)_1 \rightarrow (L+1)_2\rangle$ (0.4287)
IV	16^2B_2	6.09	0.433	$\|(H-2)_1 \rightarrow (L+1)_1\rangle$ (0.4307)
				$\|(H-2)_2 \rightarrow (L+1)_2\rangle$ (0.4270)
V	21^2A_1	6.36	0.893	$\|H-1 \rightarrow (L+1)_2\rangle$ (0.5013)
				$\|(H-2)_2 \rightarrow L+2\rangle$ (0.4747)
V	21^2B_2	6.36	0.879	$\|H-1 \rightarrow (L+1)_1\rangle$ (0.4954)
				$\|(H-2)_1 \rightarrow L+2\rangle$ (0.4701)
VI	45^2A_1	7.99	0.178	$\|Z \rightarrow L+2;\ H-1 \rightarrow (L+1)_1\rangle$ (0.4148)
				$\|(H-2)_1 \rightarrow Z;\ H-1 \rightarrow L+2\rangle$ (0.3646)
VI	45^2B_2	7.99	0.170	$\|H-1 \rightarrow L+2;\ Z \rightarrow (L+1)_2\rangle$ (0.3961)
				$\|H-1 \rightarrow Z;\ (H-2)_1 \rightarrow Z\rangle$ (0.3462)

Table XXXV: Excitation energies as obtained in the linear optical absorption spectrum of TZGND-2, from its singlet spin state, using the MRSDCI method coupled with the standard parameters in the PPP model Hamiltonian. The rest of the information is same as that in Table XXXII.

Peak	State	E (eV)	Transition Dipole (Å)	dominant contributing configurations
RS	1^1B_2			$\|Z_1, Z_2\rangle$ (0.7037)
DF	1^1A_1	0.01	-	$\|Z_1 \rightarrow Z_2\rangle$ (−0.4993)
				$\|Z_2 \rightarrow Z_1\rangle$ (0.4978)
DF	2^1B_2	1.99	-	$\|Z_1 \rightarrow L+1\rangle$ (0.4078)
				$\|H-1 \rightarrow Z_1\rangle$ (−0.3840)
I	2^1A_1	1.37	1.164	$\|Z_2 \rightarrow Z_1\rangle$ (0.5338)
				$\|Z_1 \rightarrow Z_2\rangle$ (0.5325)
II	7^1A_1	3.44	0.704	$\|(H-2)_1 \rightarrow Z_2\rangle$ (0.3631)
				$\|Z_2 \rightarrow (L+3)_1\rangle$ (−0.3607)
				$\|(H-2)_2 \rightarrow Z_1\rangle$ (0.3523)
III	12^1A_1	4.10	1.033	$\|H-3 \rightarrow Z_1\rangle$ (0.4309)
				$\|Z_1 \rightarrow L+2\rangle$ (0.4254)
III	11^1B_2	4.08	1.016	$\|H-3 \rightarrow Z_2\rangle$ (0.4321)
				$\|Z_2 \rightarrow L+2\rangle$ (0.4267)
IV	17^1B_2	5.01	0.219	$\|Z_1 \rightarrow L+1;\ Z_2 \rightarrow L+2\rangle$ (−0.3224)
				$\|H-1 \rightarrow Z_1;\ H-3 \rightarrow Z_2\rangle$ (0.3043)
V	29^1A_1	5.71	0.371	$\|H-1 \rightarrow (L+3)_1;\ Z_2 \rightarrow Z_1\rangle$ (0.2356)
				$\|(H-2)_1 \rightarrow L+1;\ Z_1 \rightarrow Z_2\rangle$ (0.2330)
V	29^1B_2	5.75	0.383	$\|H-1 \rightarrow Z_1;\ Z_2 \rightarrow L+2\rangle$ (−0.2744)
				$\|(H-2)_1 \rightarrow L+1\rangle$ (0.2731)
VI	33^1B_2	5.91	0.487	$\|H-3 \rightarrow Z_1;\ Z_2 \rightarrow L+1\rangle$ (0.2281)
				$\|H-1 \rightarrow Z_1;\ H-3 \rightarrow Z_2\rangle$ (0.2265)

Table XXXVI: Excitation energies as obtained in the linear optical absorption spectrum of TZGND-2, from its singlet spin state, using the MRSDCI method coupled with the screened parameters in the PPP model Hamiltonian. The rest of the information is same as that in Table XXXII.

Peak	State	E (eV)	Transition Dipole (Å)	dominant contributing configurations
RS	1^1A_2			$\|Z_1, Z_2\rangle$ (-0.6253)
DF	2^1B_2	2.04	-	$\|Z_1 \rightarrow L+1\rangle$ (-0.3752)
				$\|H-1 \rightarrow Z_1\rangle$ (-0.3255)
I	2^1A_1	1.13	1.491	$\|Z_1 \rightarrow Z_2\rangle$ (0.4990)
				$\|Z_2 \rightarrow Z_1\rangle$ (0.4628)
II	8^1A_1	3.41	0.761	$\|Z_1 \rightarrow (L+3)_2\rangle$ (-0.3946)
				$\|(H-2)_1 \rightarrow Z_2\rangle$ (-0.3284)
				$\|(H-2)_2 \rightarrow Z_1\rangle$ (0.3126)
II	7^1B_2	3.47	0.329	$\|Z_2 \rightarrow L+2\rangle$ (-0.3911)
				$\|Z_1 \rightarrow L+1\rangle$ (-0.3819)
III	11^1A_1	3.74	1.129	$\|H-3 \rightarrow Z_1\rangle$ (0.4310)
				$\|Z_1 \rightarrow L+2\rangle$ (-0.2734)
III	9^1B_2	3.77	1.061	$\|Z_1 \rightarrow (L+3)_1\rangle$ (0.2821)
				$\|Z_2 \rightarrow L+2\rangle$ (0.2660)
IV	28^1A_1	5.68	0.423	$\|(H-2)_2 \rightarrow (L+3)_1\rangle$ (0.2887)
				$\|H-1 \rightarrow (L+3)_2\rangle$ (0.2649)
IV	23^1B_2	5.62	0.466	$\|H-1 \rightarrow (L+3)_1\rangle$ (0.3162)
				$\|(H-2)_1 \rightarrow L+1\rangle$ (0.3084)
V	32^1A_1	5.87	0.975	$\|(H-2)_2 \rightarrow L+1\rangle$ (0.2930)
				$\|H-1 \rightarrow (L+3)_2\rangle$ (0.2562)
V	30^1B_2	5.95	0.911	$\|(H-2)_1 \rightarrow L+1\rangle$ (0.3785)
				$\|H-1 \rightarrow (L+3)_1\rangle$ (0.3120)

Table XXXVII: Excitation energies as obtained in the linear optical absorption spectrum of TZGND-2, from its triplet spin state, using the MRSDCI method coupled with the standard parameters in the PPP model Hamiltonian. The rest of the information is same as that in Table XXXII.

Peak	State	E (eV)	Transition Dipole (Å)	dominant contributing configurations
RS	1^3B_2			$\|Z_1, Z_2\rangle$ (-0.7602)
DF	1^3A_1	2.48	-	$\|H-1 \rightarrow Z_2\rangle$ (-0.5141)
				$\|Z_2 \rightarrow L+1\rangle$ (-0.5047)
DF	2^3B_2	2.31	-	$\|H-1 \rightarrow Z_1\rangle$ (0.5013)
				$\|Z_1 \rightarrow L+1\rangle$ (-0.4981)
I	5^3A_1	3.70	0.384	$\|H-1 \rightarrow Z_2\rangle$ (0.5191)
				$\|Z_2 \rightarrow L+1\rangle$ (-0.5051)
I	6^3B_2	3.66	0.322	$\|H-1 \rightarrow Z_1\rangle$ (-0.5133)
				$\|Z_1 \rightarrow L+1\rangle$ (-0.4917)
II	8^3A_1	4.29	1.354	$\|Z_1 \rightarrow L+2\rangle$ (0.4276)
				$\|H-3 \rightarrow Z_1\rangle$ (-0.4199)
II	9^3B_2	4.21	1.298	$\|Z_1 \rightarrow L+5\rangle$ (-0.2630)
				$\|H-4 \rightarrow Z_1\rangle$ (0.2539)
II	10^3B_2	4.24	0.406	$\|H-3 \rightarrow Z_2\rangle$ (0.4272)
				$\|Z_2 \rightarrow L+2\rangle$ (0.3983)
III	27^3A_1	6.22	0.938	$\|(H-2)_2 \rightarrow L+1\rangle$ (0.3368)
				$\|H-1 \rightarrow (L+3)_2\rangle$ (0.2817)
III	32^3B_2	6.25	0.502	$\|H-1 \rightarrow (L+3)_1\rangle$ (0.4317)
				$\|(H-2)_1 \rightarrow L+1\rangle$ (0.3818)
IV	34^3A_1	6.62	0.259	$\|H-1 \rightarrow Z_1; Z_2 \rightarrow (L+3)_1\rangle$ (0.2974)
				$\|(H-2)_2 \rightarrow L+1\rangle$ (0.2784)
				$\|H-1 \rightarrow (L+3)_2\rangle$ (0.2714)

Table XXXVIII: Excitation energies as obtained in the linear optical absorption spectrum of TZGND-2, from its triplet spin state, using the MRSDCI method coupled with the screened parameters in the PPP model Hamiltonian. The rest of the information is same as that in Table XXXII.

Peak	State	E (eV)	Transition Dipole (Å)	dominant contributing configurations
RS	1^3B_2			$\|Z_1, Z_2\rangle$ (-0.6607)
DF	1^3A_1	2.05	-	$\|Z_2 \rightarrow L+1\rangle$ (-0.4912)
				$\|H-1 \rightarrow Z_2\rangle$ (0.4254)
DF	2^3B_2	2.16	-	$\|Z_1 \rightarrow L+1\rangle$ (-0.4693)
				$\|H-1 \rightarrow Z_1\rangle$ (-0.4506)
I	5^3A_1	3.27	0.833	$\|H-1 \rightarrow Z_2\rangle$ (0.5133)
				$\|Z_2 \rightarrow L+1\rangle$ (0.4548)
I	6^3B_2	3.35	0.777	$\|Z_1 \rightarrow L+1\rangle$ (0.5010)
				$\|H-1 \rightarrow Z_1\rangle$ (-0.4832)
II	8^3A_1	3.98	1.232	$\|H-3 \rightarrow Z_1\rangle$ (-0.3461)
				$\|Z_1 \rightarrow L+2\rangle$ (-0.2796)
II	9^3B_2	4.03	0.862	$\|(H-2)_2 \rightarrow Z_2\rangle$ (0.4139)
				$\|Z_2 \rightarrow (L+3)_2\rangle$ (-0.3429)
				$\|Z_2 \rightarrow L+2\rangle$ (0.2283)
II	10^3B_2	4.04	1.328	$\|Z_1 \rightarrow (L+3)_1\rangle$ (0.3633)
				$\|H-3 \rightarrow Z_2\rangle$ (-0.3439)
				$\|Z_2 \rightarrow L+2\rangle$ (0.3368)
III	24^3A_1	5.48	0.876	$\|H-1 \rightarrow (L+3)_2\rangle$ (0.4243)
				$\|(H-2)_2 \rightarrow L+1\rangle$ (0.3883)
III	24^3B_2	5.47	0.786	$\|H-1 \rightarrow (L+3)_1\rangle$ (0.3786)
				$\|(H-2)_1 \rightarrow L+1\rangle$ (0.3540)
III	25^3B_2	5.51	0.493	$\|(H-2)_1 \rightarrow L+1\rangle$ (0.2945)
				$\|H-1 \rightarrow (L+3)_1\rangle$ (0.2480)
IV	35^3A_1	6.02	0.818	$\|H-1 \rightarrow (L+3)_2\rangle$ (0.4556)
				$\|(H-2)_2 \rightarrow L+1\rangle$ (0.4263)
IV	35^3B_2	6.02	0.753	$\|H-1 \rightarrow (L+3)_1\rangle$ (0.4468)
				$\|(H-2)_1 \rightarrow L+1\rangle$ (0.3641)

Table XXXIX: Excitation energies as obtained in the linear optical absorption spectrum of TZGND-3, from its doublet spin state, using the MRSDCI method coupled with the standard parameters in the PPP model Hamiltonian. The rest of the information is same as that in Table XXXII.

Peak	State	E (eV)	Transition Dipole (Å)	dominant contributing configurations
RS	1^2B_2			$\|Z_1\rangle$ (-0.5103)
				$\|Z_2 \rightarrow Z_1\rangle$ (0.4726)
				$\|Z_2 \rightarrow Z_1; (H-2)_1 \rightarrow (L+1)_1\rangle$ (0.1401)
I	2^2B_2	0.54	0.306	$\|H-1 \rightarrow Z_2\rangle$ (-0.5767)
				$\|Z_2 \rightarrow H-1\rangle$ (0.3683)
II	3^2B_2	1.52	1.241	$\|Z_2 \rightarrow H-1\rangle$ (-0.6229)
				$\|H-1 \rightarrow Z_2\rangle$ (-0.4046)
III	5^2B_2	2.74	0.174	$\|(H-2)_2 \rightarrow H-1; Z_1 \rightarrow Z_2\rangle$ (0.3761)
				$\|Z_2 \rightarrow (L+1)_2; H-1 \rightarrow Z_1\rangle$ (0.2924)
III	5^2A_1	2.78	0.069	$\|(H-2)_1 \rightarrow H-1\rangle$ (0.3321)
				$\|Z_1 \rightarrow (L+1)_2\rangle$ (0.2738)
IV	12^2B_2	3.65	0.392	$\|H-1 \rightarrow Z_1; Z_2 \rightarrow (L+1)_2\rangle$ (-0.3623)
				$\|(H-2)_2 \rightarrow Z_1; Z_2 \rightarrow H-1\rangle$ (-0.2474)
IV	12^2A_1	3.69	0.109	$\|(H-2)_1 \rightarrow Z_2; Z_1 \rightarrow H-1\rangle$ (0.2784)
				$\|(H-2)_2 \rightarrow H-1\rangle$ (0.2571)
IV	13^2A_1	3.70	0.112	$\|(H-4)_2 \rightarrow Z_1\rangle$ (0.2791)
				$\|Z_2 \rightarrow (L+1)_1\rangle$ (0.2091)

Table XL: Excitation energies as obtained in the linear optical absorption spectrum of TZGND-3, from its doublet spin state, using the MRSDCI method coupled with the standard parameters in the PPP model Hamiltonian. The table contains the information corresponding to peaks V and beyond, in continuation of the Table XXXIX. The rest of the information is same as that in Table XXXII.

Peak	State	E (eV)	Transition Dipole (Å)	dominant contributing configurations
V	15^2B_2	3.88	0.244	$\|H-1 \rightarrow (L+1)_1\rangle$ (0.2729)
				$\|Z_2 \rightarrow (L+1)_2\rangle$ (0.2245)
V	16^2B_2	3.89	0.117	$\|Z_2 \rightarrow (L+1)_2\rangle$ (0.2692)
				$\|H-3 \rightarrow Z_1\rangle$ (0.2090)
V	17^2B_2	4.07	0.356	$\|(H-2)_1 \rightarrow H-1\rangle$ (0.3335)
				$\|H-1 \rightarrow (L+1)_1\rangle$ (0.3107)
VI	24^2B_2	4.42	0.653	$\|H-1 \rightarrow (L+2)_1\rangle$ (0.2836)
				$\|(H-4)_2 \rightarrow Z_2\rangle$ (0.2128)
VI	24^2A_1	4.44	0.372	$\|Z_2 \rightarrow (L+2)_1\rangle$ (0.2665)
				$\|Z_2 \rightarrow L+3; Z_1 \rightarrow H-1\rangle$ (−0.2351)
VI	25^2B_2	4.46	0.770	$\|H-3 \rightarrow Z_1\rangle$ (0.2259)
				$\|(H-2)_1 \rightarrow Z_1\rangle$ (0.2162)
VI	25^2A_1	4.46	0.646	$\|Z_1 \rightarrow (L+2)_2\rangle$ (0.2646)
				$\|H-3 \rightarrow Z_2\rangle$ (0.2587)

Table XLI: Excitation energies as obtained in the linear optical absorption spectrum of TZGND-3, from its doublet spin state, using the MRSDCI method coupled with the screened parameters in the PPP model Hamiltonian. The rest of the information is same as that in Table XXXII.

Peak	State	E (eV)	Transition Dipole (Å)	dominant contributing configurations
RS	1^2B_2			$\|Z_1\rangle$ (−0.4547)
				$\|Z_2 \rightarrow Z_1\rangle$ (0.4059)
				$\|Z_1 \rightarrow Z_2; (H-2)_1 \rightarrow (L+1)_1\rangle$ (0.1558)
I	2^2B_2	1.23	0.523	$\|H-1 \rightarrow Z_2\rangle$ (0.5432)
				$\|Z_2 \rightarrow H-1\rangle$ (−0.3050)
II	4^2B_2	2.12	1.626	$\|Z_2 \rightarrow H-1\rangle$ (0.5850)
				$\|H-1 \rightarrow Z_2\rangle$ (0.3354)
III	6^2B_2	3.21	0.331	$\|H-1 \rightarrow Z_1; Z_2 \rightarrow (L+1)_2\rangle$ (−0.3636)
				$\|Z_1 \rightarrow Z_2; H-1 \rightarrow (L+1)_2\rangle$ (0.3356)
III	5^2A_1	3.23	0.130	$\|Z_1 \rightarrow (L+1)_2\rangle$ (0.3375)
				$\|Z_2 \rightarrow (L+1)_1; H-1 \rightarrow Z_1\rangle$ (0.2331)
IV	8^2A_1	3.56	0.179	$\|Z_1 \rightarrow (L+1)_2\rangle$ (0.4235)
				$\|(H-2)_2 \rightarrow Z_1\rangle$ (0.2743)
V	12^2B_2	4.00	0.437	$\|Z_1 \rightarrow H-1; (H-2)_2 \rightarrow Z_2\rangle$ (−0.4089)
				$\|Z_1 \rightarrow (L+1)_1\rangle$ (0.2133)
V	14^2A_1	4.06	0.358	$\|(H-2)_1 \rightarrow Z_2; Z_1 \rightarrow H-1\rangle$ (0.3465)
				$\|Z_2 \rightarrow (L+1)_1; H-1 \rightarrow Z_1\rangle$ (−0.3111)
VI	22^2A_1	4.56	0.672	$\|Z_2 \rightarrow (L+2)_1\rangle$ (0.3058)
				$\|Z_2 \rightarrow L+3\rangle$ (0.2557)
VI	22^2B_2	4.59	0.915	$\|(H-4)_1 \rightarrow Z_1\rangle$ (0.3844)
				$\|(H-4)_2 \rightarrow Z_2\rangle$ (0.2135)
VI	25^2A_1	4.67	0.803	$\|(H-4)_1 \rightarrow Z_2\rangle$ (0.3795)
				$\|Z_2 \rightarrow (L+2)_1\rangle$ (0.2828)
VI	23^2B_2	4.65	0.325	$\|Z_2 \rightarrow (L+2)_2\rangle$ (0.3412)
				$\|H-1 \rightarrow (L+2)_1\rangle$ (0.2755)

Table XLII: Excitation energies as obtained in the linear optical absorption spectrum of TZGND-3, from its quartet spin state, using the MRSDCI method coupled with the standard parameters in the PPP model Hamiltonian. The rest of the information is same as that in Table XXXII.

Peak	State	E (eV)	Transition Dipole (Å)	dominant contributing configurations
RS	1^4A_1			$\|Z_1, Z_2, H-1\rangle$ (0.7612)
DF	1^4B_2	2.52	-	$\|(H-2)_1 \rightarrow H-1\rangle$ (0.4741)
				$\|H-1 \rightarrow (L+1)_1\rangle$ (0.3642)
I	2^4A_1	2.67	0.182	$\|(H-2)_2 \rightarrow H-1\rangle$ (0.3514)
				$\|(H-2)_1 \rightarrow Z_2\rangle$ (0.3004)
II	5^4A_1	3.46	0.257	$\|H-3 \rightarrow Z_2\rangle$ (0.3557)
				$\|(H-4)_2 \rightarrow Z_1\rangle$ (−0.3263)
II	6^4B_2	3.44	0.314	$\|(H-2)_1 \rightarrow H-1\rangle$ (−0.4566)
				$\|Z_2 \rightarrow (L+1)_2\rangle$ (0.3216)
III	9^4A_1	3.86	0.980	$\|H-1 \rightarrow (L+1)_2\rangle$ (−0.3703)
				$\|Z_2 \rightarrow (L+1)_1\rangle$ (0.3648)
III	9^4B_2	3.81	0.983	$\|Z_2 \rightarrow (L+1)_2\rangle$ (−0.4144)
				$\|H-1 \rightarrow (L+1)_1\rangle$ (0.2990)
IV	13^4A_1	4.37	1.786	$\|H-1 \rightarrow (L+2)_2\rangle$ (0.2985)
				$\|Z_2 \rightarrow (L+2)_1\rangle$ (0.2871)
IV	13^4B_2	4.33	1.801	$\|H-1 \rightarrow (L+2)_1\rangle$ (−0.2867)
				$\|Z_2 \rightarrow (L+2)_2\rangle$ (−0.2864)
V	18^4A_1	4.80	0.216	$\|Z_1 \rightarrow (L+2)_2\rangle$ (0.3653)
				$\|Z_2 \rightarrow L+3\rangle$ (−0.3593)
V	16^4B_2	4.72	0.406	$\|Z_1 \rightarrow (L+2)_1\rangle$ (0.4397)
				$\|H-1 \rightarrow L+3\rangle$ (−0.3794)

Table XLIII: Excitation energies as obtained in the linear optical absorption spectrum of TZGND-3, from its quartet spin state, using the MRSDCI method coupled with the screened parameters in the PPP model Hamiltonian. The rest of the information is same as that in Table XXXII.

Peak	State	E (eV)	Transition Dipole (Å)	dominant contributing configurations
RS	1^4A_1			$\|Z_1, Z_2, H-1\rangle$ (0.6762)
DF	2^4A_1	2.39	-	$\|H-1 \rightarrow (L+1)_2\rangle$ (−0.3333)
				$\|(H-2)_2 \rightarrow H-1\rangle$ (−0.3084)
I	1^4B_2	1.98	0.427	$\|H-1 \rightarrow (L+1)_1\rangle$ (0.5920)
				$\|(H-2)_1 \rightarrow H-1\rangle$ (−0.2485)
II	9^4A_1	3.30	1.729	$\|H-1 \rightarrow (L+2)_2\rangle$ (0.4783)
				$\|(H-4)_2 \rightarrow H-1\rangle$ (0.2996)
II	8^4B_2	3.17	1.740	$\|(H-2)_2 \rightarrow Z_2\rangle$ (−0.4334)
				$\|Z_2 \rightarrow (L+1)_2\rangle$ (−0.3567)
III	13^4A_1	3.86	1.591	$\|H-3 \rightarrow Z_2\rangle$ (−0.4467)
				$\|Z_2 \rightarrow L+3\rangle$ (0.3104)
III	14^4B_2	3.87	1.726	$\|H-3 \rightarrow H-1\rangle$ (0.4094)
				$\|(H-4)_1 \rightarrow Z_1\rangle$ (0.2862)

Table XLIV: Excitation energies as obtained in the linear optical absorption spectrum of TZGND-4, from its singlet spin state, using the MRSDCI method coupled with the standard parameters in the PPP model Hamiltonian. The rest of the information is same as that in Table XXXII.

Peak	State	E (eV)	Transition Dipole (Å)	dominant contributing configurations
RS	1^1B_2			$\|(H-2)_1,(H-2)_2\rangle$ (0.3823)
				$\|(H-2)_1 \rightarrow H-1\rangle$ (0.3464)
				$\|Z \rightarrow (H-2)_1; Z \rightarrow H-1\rangle$ (−0.3126)
I	1^1A_1	0.27	0.883	$\|Z \rightarrow H-1\rangle$ (0.5216)
				$\|Z \rightarrow (H-2)_2; Z \rightarrow H-1\rangle$ (−0.3248)
				$\|Z \rightarrow (H-2)_1\rangle$ (0.3239)
II	3^1A_1	0.80	0.614	$\|(H-2)_1 \rightarrow (H-2)_2\rangle$ (0.4833)
				$\|(H-2)_2 \rightarrow (H-2)_1\rangle$ (−0.3753)
	2^1B_2	0.77	0.542	$\|(H-2)_1 \rightarrow (H-2)_2\rangle$ (−0.4332)
				$\|Z \rightarrow (H-2)_2; (H-2)_1 \rightarrow H-1\rangle$ (−0.4109)
				$\|Z \rightarrow (H-2)_2\rangle$ (0.2701)
III	4^1B_2	1.03	0.943	$\|Z \rightarrow H-1; Z \rightarrow H-1\rangle$ (−0.4985)
				$\|(H-2)_1 \rightarrow H-1\rangle$ (−0.3931)
IV	4^1A_1	1.56	0.315	$\|Z \rightarrow (H-2)_2; Z \rightarrow H-1\rangle$ (−0.5258)
				$\|Z \rightarrow (H-2)_1\rangle$ (−0.3249)
V	5^1A_1	1.89	0.688	$\|Z \rightarrow H-1\rangle$ (0.6576)
				$\|(H-2)_1 \rightarrow (H-2)_2\rangle$ (0.2797)
VI	6^1A_1	2.19	0.723	$\|Z \rightarrow (H-2)_1\rangle$ (−0.4417)
				$\|Z \rightarrow (H-2)_2; Z \rightarrow H-1\rangle$ (0.3309)
VII	7^1A_1	2.75	0.634	$\|(H-2)_2 \rightarrow (H-2)_1\rangle$ (−0.3456)
				$\|(H-2)_1 \rightarrow (H-2)_2\rangle$ (−0.3341)
VIII	8^1B_2	3.17	0.917	$\|Z \rightarrow (H-2)_2; (H-3)_1 \rightarrow H-1\rangle$ (0.5027)
				$\|(H-3)_2 \rightarrow (H-2)_2\rangle$ (−0.3004)
				$\|Z \rightarrow (H-2)_2; H-4 \rightarrow H-1\rangle$ (0.2648)

Table XLV: Excitation energies as obtained in the linear optical absorption spectrum of TZGND-4, from its singlet spin state, using the MRSDCI method coupled with the standard parameters in the PPP model Hamiltonian. The table contains the information corresponding to peaks IX and beyond, in continuation of the Table XLIV. The rest of the information is same as that in Table XXXII.

Peak	State	E (eV)	Transition Dipole (Å)	dominant contributing configurations
IX	9^1A_1	3.54	0.405	$\|Z \rightarrow (H-2)_2; Z \rightarrow (L+1)_1\rangle$ (0.4707)
				$\|Z \rightarrow (H-2)_1; Z \rightarrow (L+1)_2\rangle$ (−0.4148)
	10^1B_2	3.53	0.800	$\|(H-3)_2 \rightarrow (H-2)_2\rangle$ (0.4607)
				$\|Z \rightarrow (H-2)_2; (H-3)_1 \rightarrow H-1\rangle$ (0.3077)
				$\|Z \rightarrow (L+1)_2\rangle$ (0.2047)
X	15^1B_2	4.05	0.349	$\|Z \rightarrow (H-2)_2; (H-5)_1 \rightarrow H-1\rangle$ (0.3082)
				$\|Z \rightarrow (H-2)_2; (H-3)_1 \rightarrow H-1\rangle$ (0.2837)
				$\|Z \rightarrow (H-2)_1; (H-2)_2 \rightarrow H-1\rangle$ (−0.2673)
XI	19^1B_2	4.53	0.541	$\|Z \rightarrow (H-2)_2; H-4 \rightarrow H-1\rangle$ (0.2729)
				$\|Z \rightarrow (H-2)_2; (H-3)_1 \rightarrow H-1\rangle$ (0.2242)
				$\|Z \rightarrow (H-2)_2; (H-5)_1 \rightarrow H-1\rangle$ (0.3082)
XII	17^1A_1	4.65	0.244	$\|Z \rightarrow (H-2)_2; Z \rightarrow (H-2)_1; (H-3)_1 \rightarrow H-1\rangle$ (0.2978)
				$\|Z \rightarrow H-1; (H-2)_1 \rightarrow H-1\rangle$ (−0.2155)
				$\|Z \rightarrow (H-2)_2; Z \rightarrow (H-2)_1; (H-5)_1 \rightarrow H-1\rangle$ (0.2049)
	21^1B_2	4.65	0.232	$\|Z \rightarrow (H-2)_2; (H-5)_1 \rightarrow H-1\rangle$ (0.4845)
				$\|Z \rightarrow H-1; (H-2)_2 \rightarrow H-1\rangle$ (0.2501)
				$\|Z \rightarrow (H-2)_2; H-4 \rightarrow H-1\rangle$ (0.1947)
XIII	29^1B_2	5.06	0.770	$\|Z \rightarrow (H-2)_2; Z \rightarrow H-1; (H-3)_2 \rightarrow H-1\rangle$ (0.2611)
				$\|Z \rightarrow H-1; Z \rightarrow H-1; (H-3)_1 \rightarrow (H-2)_1\rangle$ (0.2336)

Table XLVI: Excitation energies as obtained in the linear optical absorption spectrum of TZGND-4, from its singlet spin state, using the MRSDCI method coupled with the screened parameters in the PPP model Hamiltonian. The rest of the information is same as that in Table XXXII.

Peak	State	E (eV)	Transition Dipole (Å)	dominant contributing configurations
RS	1^1B_2			$\|(H-2)_1,(H-2)_2\rangle$ (0.3823)
				$\|Z\rightarrow(H-2)_2\rangle$ (−0.4316)
				$\|Z\rightarrow(H-2)_2;(H-2)_1\rightarrow H-1\rangle$ (−0.1571)
I	1^1A_1	0.50	2.004	$\|Z\rightarrow(H-2)_1;Z\rightarrow(H-2)_2\rangle$ (−0.6305)
				$\|Z\rightarrow(H-2)_1;Z\rightarrow(H-2)_2;(H-3)_2\rightarrow(L+1)_2\rangle$ (−0.1757)
	2^1B_2	0.46	0.408	$\|Z\rightarrow(H-2)_2;(H-2)_1\rightarrow H-1\rangle$ (−0.5558)
				$\|Z\rightarrow(H-2)_2\rangle$ (−0.2805)
II	3^1A_1	1.07	0.458	$\|Z\rightarrow(H-2)_1\rangle$ (−0.5558)
				$\|Z\rightarrow(H-2)_2;Z\rightarrow H-1\rangle$ (−0.4122)
	3^1B_2	1.10	0.419	$\|Z\rightarrow(H-2)_2\rangle$ (−0.4834)
				$\|Z\rightarrow(H-2)_2;(H-2)_1\rightarrow H-1\rangle$ (0.2667)
III	4^1B_2	1.89	0.975	$\|Z\rightarrow(L+1)_2\rangle$ (−0.5137)
				$\|Z\rightarrow(H-2)_2;Z\rightarrow(L+1)_2\rangle$ (0.4568)
IV	4^1A_1	2.43	1.027	$\|Z\rightarrow(H-2)_2;Z\rightarrow(L+1)_1\rangle$ (−0.5604)
				$\|Z\rightarrow(H-2)_1;Z\rightarrow(L+1)_2\rangle$ (−0.4270)
V	8^1B_2	2.69	0.697	$\|Z\rightarrow(H-2)_2;(H-3)_1\rightarrow H-1\rangle$ (0.4329)
				$\|Z\rightarrow(H-2)_2;(H-2)_1\rightarrow(L+1)_1\rangle$ (0.3090)
VI	12^1B_2	3.33	1.588	$\|Z\rightarrow(H-2)_2;(H-3)_1\rightarrow H-1\rangle$ (0.4448)
				$\|Z\rightarrow(H-2)_2;(H-5)_1\rightarrow H-1\rangle$ (0.2111)
VII	13^1B_2	3.78	1.052	$\|Z\rightarrow(H-2)_2;(H-5)_1\rightarrow H-1\rangle$ (0.6611)
				$\|Z\rightarrow(H-2)_2;(H-3)_1\rightarrow H-1;(H-7)_1\rightarrow(L+1)_1\rangle$ (0.1717)
VIII	10^1A_1	4.09	0.738	$\|Z\rightarrow(H-2)_2;H-6\rightarrow(H-2)_1\rangle$ (−0.4998)
				$\|Z\rightarrow(H-2)_1;Z\rightarrow(L+5)_2\rangle$ (−0.3125)
IX	11^1A_1	4.28	0.923	$\|Z\rightarrow H-1\rangle$ (0.6320)
				$\|Z\rightarrow(H-2)_2;Z\rightarrow(L+5)_1\rangle$ (0.6320)
X	12^1A_1	4.59	1.624	$\|Z\rightarrow H-1\rangle$ (0.6198)
				$\|Z\rightarrow(H-2)_2;(H-2)_1\rightarrow H-1;Z\rightarrow H-1\rangle$ (0.3492)
				$\|(H-2)_2\rightarrow(H-2)_1\rangle$ (0.2313)

Table XLVII: Excitation energies as obtained in the linear optical absorption spectrum of TZGND-4, from its triplet spin state, using the MRSDCI method coupled with the standard parameters in the PPP model Hamiltonian. The rest of the information is same as that in Table XXXII.

Peak	State	E (eV)	Transition Dipole (Å)	dominant contributing configurations
RS	1^3A_1			$\|Z, H-1, (H-2)_1, (H-2)_2\rangle$ (0.4404)
				$\|(H-2)_2 \rightarrow Z\rangle$ (−0.3988)
				$\|Z \rightarrow (H-2)_2\rangle$ (−0.3822)
I	3^3B_2	1.17	0.770	$\|Z \rightarrow H-1\rangle$ (−0.7595)
				$\|Z \rightarrow H-1; (H-3)_2 \rightarrow (L+1)_2\rangle$ (0.1567)
II	5^3A_1	1.78	0.313	$\|(H-2)_2 \rightarrow Z\rangle$ (−0.4612)
				$\|Z \rightarrow (H-2)_2\rangle$ (−0.4520)
				$\|H-1 \rightarrow (H-2)_1\rangle$ (−0.3087)
				$\|(H-2)_1 \rightarrow H-1\rangle$ (−0.1968)
III	5^3B_2	2.27	0.242	$\|(H-2)_1 \rightarrow (H-2)_2\rangle$ (−0.5948)
				$\|H-1 \rightarrow (H-2)_2\rangle$ (0.3095)
				$\|(H-3)_1 \rightarrow (H-2)_2\rangle$ (0.2007)
IV	6^3B_2	3.04	1.100	$\|H-1 \rightarrow Z\rangle$ (−0.7144)
				$\|H-4 \rightarrow Z\rangle$ (0.1883)
V	9^3A_1	3.41	0.308	$\|Z \rightarrow (H-2)_2; (H-3)_1 \rightarrow H-1\rangle$ (−0.4238)
				$\|Z \rightarrow (H-2)_2; H-1 \rightarrow (L+1)_1\rangle$ (0.3693)
				$\|(H-3)_2 \rightarrow (H-2)_2\rangle$ (0.2859)
	7^3B_2	3.45	0.239	$\|(H-2)_2 \rightarrow H-1\rangle$ (0.4621)
				$\|(H-3)_1 \rightarrow (H-2)_2\rangle$ (0.3244)
				$\|H-4 \rightarrow (H-2)_2\rangle$ (0.2749)
				$\|(H-5)_1 \rightarrow (H-2)_2\rangle$ (0.2252)
VI	11^3A_1	3.71	0.384	$\|Z \rightarrow (L+1)_2\rangle$ (0.4578)
				$\|(H-3)_2 \rightarrow (H-2)_2\rangle$ (−0.2524)
	8^3B_2	3.75	0.333	$\|(H-3)_1 \rightarrow (H-2)_2\rangle$ (0.5437)
				$\|H-1 \rightarrow (L+1)_2; Z \rightarrow (H-2)_2\rangle$ (0.3079)
				$\|(H-2)_2 \rightarrow H-1\rangle$ (−0.2784)

Table XLVIII: Excitation energies as obtained in the linear optical absorption spectrum of TZGND-4, from its triplet spin state, using the MRSDCI method coupled with the standard parameters in the PPP model Hamiltonian. The table contains the information corresponding to peaks VII and beyond, in continuation of the Table XLVII. The rest of the information is same as that in Table XXXII.

Peak	State	E (eV)	Transition Dipole (Å)	dominant contributing configurations
VII	13^3A_1	3.96	0.403	$\|(H-3)_2 \rightarrow (H-2)_2\rangle$ (0.5633)
				$\|Z \rightarrow (L+1)_2\rangle$ (0.1924)
	10^3B_2	3.98	0.368	$\|(H-5)_1 \rightarrow (H-2)_2\rangle$ (0.3996)
				$\|H-4 \rightarrow (H-2)_2\rangle$ (0.3895)
				$\|H-1 \rightarrow (L+1)_2; Z \rightarrow (H-2)_2\rangle$ (−0.2843)
VIII	19^3A_1	4.47	0.951	$\|(H-3)_2 \rightarrow (H-2)_2\rangle$ (0.2859)
				$\|H-6 \rightarrow (H-2)_2\rangle$ (0.2534)
				$\|Z \rightarrow (H-2)_2; H-1 \rightarrow (L+1)_1\rangle$ (0.2343)
	13^3B_2	4.46	0.227	$\|(H-3)_1 \rightarrow (H-2)_2\rangle$ (0.3749)
				$\|(H-5)_1 \rightarrow (H-2)_2\rangle$ (0.3307)
IX	23^3A_1	4.78	0.262	$\|H-1 \rightarrow (L+1)_1\rangle$ (0.3112)
				$\|Z \rightarrow L+3\rangle$ (0.2524)
				$\|H-6 \rightarrow (H-2)_2\rangle$ (0.2304)
X	28^3A_1	4.99	1.012	$\|Z \rightarrow L+3\rangle$ (0.3633)
				$\|(H-3)_1 \rightarrow H-1\rangle$ (0.2344)
				$\|(H-3)_2 \rightarrow Z\rangle$ (0.2010)
XI	22^3B_2	5.27	0.332	$\|Z \rightarrow L+2\rangle$ (0.2319)
				$\|H-4 \rightarrow Z\rangle$ (0.2254)
XII	28^3B_2	5.62	0.275	$\|(H-3)_1 \rightarrow Z\rangle$ (0.2228)
				$\|Z \rightarrow (L+1)_1\rangle$ (0.2026)

Table XLIX: Excitation energies as obtained in the linear optical absorption spectrum of TZGND-4, from its triplet spin state, using the MRSDCI method coupled with the screened parameters in the PPP model Hamiltonian. The rest of the information is same as that in Table XXXII.

Peak	State	E (eV)	Transition Dipole (Å)	dominant contributing configurations
RS	1^3A_1			$\|H-1,(H-2)_1\rangle$ (0.5038)
				$\|(H-2)_2 \rightarrow Z\rangle$ (0.4344)
I	2^3A_1	0.24	0.842	$\|(H-2)_2 \rightarrow Z\rangle$ (0.6859)
				$\|(H-3)_2 \rightarrow Z;(H-2)_2 \rightarrow (L+1)_2\rangle$ (0.1792)
	1^3B_2	0.28	0.629	$\|H-1 \rightarrow Z\rangle$ (0.6053)
				$\|(H-2)_1 \rightarrow Z\rangle$ (0.2568)
II	3^3A_1	0.72	1.283	$\|(H-2)_2 \rightarrow Z\rangle$ (0.6666)
				$\|(H-3)_2 \rightarrow Z;(H-2)_2 \rightarrow (L+1)_2\rangle$ (0.1734)
III	4^3B_2	2.16	1.001	$\|H-4 \rightarrow (L+1)_2;(H-2)_2 \rightarrow Z\rangle$ (0.4270)
				$\|H-4 \rightarrow Z;(H-2)_2 \rightarrow Z\rangle$ (0.3877)
				$\|H-4 \rightarrow (L+1)_2\rangle$ (0.3648)
IV	6^3A_1	2.46	0.681	$\|(H-2)_2 \rightarrow (L+1)_2\rangle$ (0.5197)
				$\|(H-2)_2 \rightarrow L+3\rangle$ (0.4133)
				$\|(H-3)_2 \rightarrow Z\rangle$ (0.1483)
V	10^3A_1	2.80	0.965	$\|(H-3)_2 \rightarrow Z\rangle$ (0.4987)
				$\|(H-3)_1 \rightarrow H-1\rangle$ (−0.2726)
				$\|(H-2)_2 \rightarrow (L+1)_2\rangle$ (0.2452)
VI	13^3A_1	3.01	1.367	$\|(H-3)_1 \rightarrow H-1\rangle$ (−0.4924)
				$\|(H-2)_1 \rightarrow (L+1)_1\rangle$ (0.2970)
				$\|(H-2)_2 \rightarrow (L+4)_2\rangle$ (0.2214)
	11^3B_2	3.05	0.274	$\|H-4 \rightarrow Z\rangle$ (0.3523)
				$\|H-1 \rightarrow L+3;(H-2)_2 \rightarrow Z\rangle$ (0.3005)
				$\|(H-3)_1 \rightarrow Z\rangle$ (0.2993)

Table L: Excitation energies as obtained in the linear optical absorption spectrum of TZGND-4, from its triplet spin state, using the MRSDCI method coupled with the screened parameters in the PPP model Hamiltonian. The table contains the information corresponding to peaks VII and beyond, in continuation of the Table XLIX. The rest of the information is same as that in Table XXXII.

Peak	State	E (eV)	Transition	dominant contributing configurations
			Dipole (Å)	
VII	17^3A_1	3.39	1.404	$\|(H-3)_2 \rightarrow Z\rangle$ (0.4536)
				$\|(H-2)_2 \rightarrow (L+4)_2\rangle$ (0.3902)
VIII	24^3A_1	4.02	0.524	$\|H-6 \rightarrow Z\rangle$ (0.4929)
				$\|(H-2)_2 \rightarrow L+8\rangle$ (0.2968)
IX	25^3A_1	4.24	0.682	$\|(H-2)_2 \rightarrow Z; (H-2)_2 \rightarrow Z\rangle$ (−0.4039)
				$\|(H-2)_1 \rightarrow (L+4)_1\rangle$ (0.3073)
X	29^3A_1	4.69	0.724	$\|H-1 \rightarrow (H-2)_1; (H-2)_2 \rightarrow Z\rangle$ (0.5374)
				$\|(H-2)_1 \rightarrow H-1; (H-2)_2 \rightarrow Z\rangle$ (0.5001)
XI	30^3A_1	5.13	0.335	$\|(H-2)_2 \rightarrow (L+5)_2\rangle$ (0.5423)
				$\|(H-3)_2 \rightarrow (L+1)_2; (H-2)_2 \rightarrow (L+5)_2\rangle$ (0.1855)

Table LI: Excitation energies as obtained in the linear optical absorption spectrum of TZGND-4, from its quintet spin state, using the MRSDCI method coupled with the standard parameters in the PPP model Hamiltonian. The rest of the information is same as that in Table XXXII.

Peak	State	E (eV)	Transition Dipole (Å)	dominant contributing configurations
RS	1^5A_1			$\|Z, H-1, (H-2)_1, (H-2)_2\rangle$ (0.7631)
I	2^5A_1	2.68	0.583	$\|(H-3)_1 \rightarrow H-1\rangle$ (−0.5433)
				$\|(H-3)_2 \rightarrow Z\rangle$ (0.4735)
				$\|H-1 \rightarrow (L+1)_1\rangle$ (0.2328)
	3^5B_2	2.68	0.500	$\|Z \rightarrow (L+1)_1\rangle$ (0.5121)
				$\|H-1 \rightarrow (L+1)_2\rangle$ (−0.4569)
				$\|(H-3)_1 \rightarrow Z\rangle$ (−0.3170)
				$\|(H-3)_2 \rightarrow H-1\rangle$ (0.1358)
II	3^5A_1	3.20	0.455	$\|(H-3)_2 \rightarrow Z\rangle$ (0.4874)
				$\|(H-3)_1 \rightarrow H-1\rangle$ (0.4101)
				$\|Z \rightarrow (L+1)_2\rangle$ (−0.3050)
				$\|H-1 \rightarrow (L+1)_1\rangle$ (−0.2814)
	4^5B_2	3.20	0.194	$\|(H-2)_2 \rightarrow (L+1)_1\rangle$ (0.6363)
				$\|Z \rightarrow L+2\rangle$ (−0.3309)
III	6^5A_1	3.69	2.151	$\|H-1 \rightarrow (L+1)_1\rangle$ (−0.3353)
				$\|Z \rightarrow (L+1)_2\rangle$ (−0.3349)
				$\|(H-5)_1 \rightarrow H-1\rangle$ (−0.3073)
				$\|(H-3)_1 \rightarrow H-1\rangle$ (−0.2365)
				$\|Z \rightarrow (L+4)_2\rangle$ (−0.2351)
				$\|(H-2)_2 \rightarrow L+3\rangle$ (−0.2213)
				$\|(H-3)_2 \rightarrow Z\rangle$ (−0.2045)
	6^5B_2	3.69	1.528	$\|H-1 \rightarrow (L+1)_2\rangle$ (−0.5279)
				$\|Z \rightarrow (L+1)_1\rangle$ (−0.3550)
				$\|(H-3)_2 \rightarrow H-1\rangle$ (0.3165)
				$\|(H-3)_1 \rightarrow Z\rangle$ (0.2862)

Table LII: Excitation energies as obtained in the linear optical absorption spectrum of TZGND-4, from its quintet spin state, using the MRSDCI method coupled with the standard parameters in the PPP model Hamiltonian. The table contains the information corresponding to peaks IV and beyond, in continuation of the Table LI. The rest of the information is same as that in Table XXXII.

Peak	State	E (eV)	Transition Dipole (Å)	dominant contributing configurations
IV	7^5B_2	4.01	0.736	$\|Z \rightarrow L+2\rangle$ (-0.6571)
				$\|(H-2)_2 \rightarrow (L+1)_1\rangle$ (-0.2964)
V	9^5B_2	4.39	1.310	$\|(H-3)_1 \rightarrow (H-2)_2\rangle$ (0.5593)
				$\|H-4 \rightarrow Z\rangle$ (0.2923)
VI	11^5B_2	4.69	0.486	$\|(H-5)_2 \rightarrow H-1\rangle$ (-0.4373)
				$\|(H-3)_2 \rightarrow H-1\rangle$ (0.2572)
VII	11^5A_1	5.46	0.547	$\|(H-5)_2 \rightarrow Z\rangle$ (0.4260)
				$\|(H-2)_1 \rightarrow L+2\rangle$ (0.3091)
				$\|Z \rightarrow (L+4)_2\rangle$ (0.2652)
VIII	16^5A_1	5.86	0.240	$\|H-1 \rightarrow L+2\rangle$ (-0.4824)
				$\|(H-3)_2 \rightarrow (H-2)_2\rangle$ (-0.2911)
				$\|Z \rightarrow L+3\rangle$ (-0.2891)
	20^5B_2	5.86	0.899	$\|(H-3)_2 \rightarrow (L+1)_1\rangle$ (0.3291)
				$\|(H-5)_1 \rightarrow Z\rangle$ (-0.2687)
				$\|(H-3)_1 \rightarrow (H-2)_2\rangle$ (-0.2215)
IX	24^5A_1	6.41	0.713	$\|H-4 \rightarrow (H-2)_1\rangle$ (-0.3665)
				$\|(H-9)_1 \rightarrow H-1\rangle$ (-0.3612)
				$\|H-1 \rightarrow L+7\rangle$ (0.2122)
	25^5B_2	6.41	0.446	$\|(H-9)_2 \rightarrow H-1\rangle$ (-0.2994)
				$\|Z \rightarrow (L+10)_1\rangle$ (-0.2267)
				$\|Z \rightarrow (L+6)_1\rangle$ (-0.2246)

Table LIII: Excitation energies as obtained in the linear optical absorption spectrum of TZGND-4, from its quintet spin state, using the MRSDCI method coupled with the screened parameters in the PPP model Hamiltonian. The rest of the information is same as that in Table XXXII.

Peak	State	E (eV)	Transition Dipole (Å)	dominant contributing configurations
RS	1^5A_1			$\|Z, H-1, (H-2)_1, (H-2)_2\rangle$ (0.7631)
I	1^5B_2	1.95	1.177	$\|Z \rightarrow (L+1)_1\rangle$ (0.6673)
				$\|Z \rightarrow (L+1)_1; (H-3)_1 \rightarrow (L+1)_1\rangle$ (0.2394)
				$\|Z \rightarrow (L+1)_1; (H-3)_2 \rightarrow (L+1)_2\rangle$ (0.1689)
II	5^5A_1	2.81	2.322	$\|(H-3)_1 \rightarrow H-1\rangle$ (0.4006)
				$\|H-1 \rightarrow (L+1)_1\rangle$ (0.3942)
				$\|Z \rightarrow (L+1)_2\rangle$ (−0.2950)
				$\|(H-3)_2 \rightarrow Z\rangle$ (0.2792)
III	8^5A_1	3.41	0.805	$\|H-4 \rightarrow (H-2)_1\rangle$ (−0.4386)
				$\|(H-5)_2 \rightarrow Z\rangle$ (0.3226)
				$\|(H-2)_1 \rightarrow L+2\rangle$ (−0.3118)
				$\|(H-5)_1 \rightarrow H-1\rangle$ (0.2053)
				$\|Z \rightarrow (L+5)_2\rangle$ (0.1485)
IV	11^5A_1	3.71	0.952	$\|(H-5)_1 \rightarrow H-1\rangle$ (−0.3656)
				$\|(H-5)_2 \rightarrow Z\rangle$ (0.3226)
				$\|Z \rightarrow (L+4)_2\rangle$ (−0.2854)
				$\|(H-2)_1 \rightarrow (L+4)_1\rangle$ (−0.2528)
				$\|(H-2)_2 \rightarrow (L+4)_2\rangle$ (−0.2488)
V	5^5B_2	4.16	0.339	$\|Z \rightarrow L+7\rangle$ (0.6902)
				$\|Z \rightarrow (L+1)_1; (H-3)_1 \rightarrow L+7\rangle$ (0.1906)
				$\|Z \rightarrow (L+1)_2; (H-3)_2 \rightarrow L+7\rangle$ (0.1778)
VI	11^5B_2	5.47	0.967	$\|(H-3)_2 \rightarrow H-1\rangle$ (−0.6627)
				$\|(H-3)_2 \rightarrow (L+1)_1; (H-3)_1 \rightarrow H-1\rangle$ (0.3088)
				$\|Z \rightarrow (L+5)_1\rangle$ (0.1514)
VII	27^5A_1	6.62	0.403	$\|(H-2)_2 \rightarrow L+3\rangle$ (−0.5010)
				$\|(H-7)_2 \rightarrow Z\rangle$ (0.3062)
				$\|Z \rightarrow L+8\rangle$ (0.2096)
	20^5B_2	6.62	1.066	$\|(H-2)_2 \rightarrow (L+4)_1\rangle$ (0.3958)
				$\|H-6 \rightarrow (H-2)_1\rangle$ (0.3508)

[1] K. Gundra and A. Shukla, Phys. Rev. B **83**, 075413 (2011).

[2] K. S. Novoselov, A. K. Geim, S. V. Morozov, D. Jiang, Y. Zhang, S. V. Dubonos, I. V. Grigorieva, and A. A. Firsov, Science **306**, 666 (2004).

[3] K. S. Novoselov, Z. Jiang, Y. Zhang, S. V. Morozov, H. L. Stormer, U. Zeitler, J. C. Maan, G. S. Boebinger, P. Kim, and A. K. Geim, Science **315**, 1379 (2007).

[4] A. H. Castro Neto, F. Guinea, N. M. R. Peres, K. S. Novoselov, and A. K. Geim, Rev. Mod. Phys. **81**, 109 (2009).

[5] J. Fernández-Rossier and J. J. Palacios, Phys. Rev. Lett. **99**, 177204 (2007).

[6] M. Ezawa, Phys. Rev. B **77**, 155411 (2008).

[7] M. Kinza, J. Ortloff, and C. Honerkamp, Phys. Rev. B **82**, 155430 (2010).

[8] A. D. Güçlü, P. Potasz, and P. Hawrylak, Phys. Rev. B **82**, 155445 (2010).

[9] M. Ezawa, Phys. Rev. B **79**, 241407 (2009).

[10] W. L. Wang, O. V. Yazyev, S. Meng, and E. Kaxiras, Phys. Rev. Lett. **102**, 157201 (2009).

[11] J. Akola, H. P. Heiskanen, and M. Manninen, Phys. Rev. B **77**, 193410 (2008).

[12] O. V. Yazyev, Rep. Progr. Phys. **73**, 056501 (2010).

[13] W. Leupin and J. Wirz, Journal of the American Chemical Society **102**, 6068 (1980).

[14] J. Inoue, K. Fukui, T. Kubo, S. Nakazawa, K. Sato, D. Shiomi, Y. Morita, K. Yamamoto, T. Takui, and K. Nakasuji, J. Am. Chem. Soc. **123**, 12702 (2001).

[15] G. Allinson, R. J. Bushby, J.-L. Paillaud, and M. Thornton-Pett, J. Chem. Soc., Perkin Trans. 1 **4**, 385 (1995).

[16] T. Yamamoto, T. Noguchi, and K. Watanabe, Phys. Rev. B **74**, 121409 (2006).

[17] M. Ezawa, Phys. Rev. B **76**, 245415 (2007).

[18] M. R. Philpott, F. Cimpoesu, and Y. Kawazoe, Chem. Phys. **354**, 1 (2008).

[19] M. Ghaffarian and F. Ebrahimi, Phys. Scripta **88**, 025703 (2013).

[20] K. Yoneda, M. Nakano, R. Kishi, H. Takahashi, A. Shimizu, T. Kubo, K. Kamada, K. Ohta, B. Champagne, and E. Botek, Chem. Phys. Lett. **480**, 278 (2009).

[21] H. Nagai, M. Nakano, K. Yoneda, R. Kishi, H. Takahashi, A. Shimizu, T. Kubo, K. Kamada, K. Ohta, E. Botek, and B. Champagne, Chem. Phys. Lett. **489**, 212 (2010).

[22] M. Ezawa, J. Nanosci. Nanotechnol. **12**, 386 (2012).

[23] I. Romanovsky, C. Yannouleas, and U. Landman, Phys. Rev. B **86**, 165440 (2012).

[24] A. A. Nila, G. Alexandru Nemnes, and A. Manolescu, arXiv:1411.6042 (2014).

[25] Q.-R. Dong, RSC Adv. **4**, 12287 (2014).

[26] W. Wang, T. Christensen, A.-P. Jauho, K. S. Thygesen, M. Wubs, and N. A. Mortensen, Sci. Rep. **5**, 9535 (2015).

[27] T. Basak, H. Chakraborty, and A. Shukla, Phys. Rev. B **92**, 205404 (2015).

[28] S. Mikhailov, *Physics and applications of graphene-theory* (INTECH Open Access, Croatia, 2011) pp. 243–276.

[29] E. H. Lieb, Phys. Rev. Lett. **62**, 1201 (1989).

[30] H. G. Kiess and D. Baeriswyl, *Conjugated Conducting Polymers* (Springer-Verlag, London, 1992).

[31] A. Shukla, Chem. Phys. **300**, 177 (2004).

[32] A. Shukla, Phys. Rev. B **69**, 165218 (2004).

[33] A. Shukla, Phys. Rev. B **65**, 125204 (2002).

[34] P. Sony and A. Shukla, Phys. Rev. B **75**, 155208 (2007).

[35] P. Sony and A. Shukla, J. Chem. Phys. **131**, 014302 (2009).

[36] H. Chakraborty and A. Shukla, J. Phys. Chem. A **117**, 14220 (2013).

[37] P. Sony and A. Shukla, Comput. Phys. Commun. **181**, 821 (2010).

[38] H. Chakraborty and A. Shukla, J. Chem. Phys. **141**, 164301 (2014).

[39] L. V. Slipchenko, T. E. Munsch, P. G. Wenthold, and A. I. Krylov, Angew. Chem. Int. Ed. **43**, 742 (2004).